LBL-34734
UC-122
Preprint

Lawrence Berkeley Laboratory

UNIVERSITY OF CALIFORNIA

EARTH SCIENCES DIVISION

Submitted to Geophysics

Crosshole Electromagnetic Imaging for Reservoir Definition and Monitoring

M.J. Wilt, D.L. Alumbaugh, H.F. Morrison, A. Becker, K.H. Lee, and M. Deszcz-Pan

July 1993

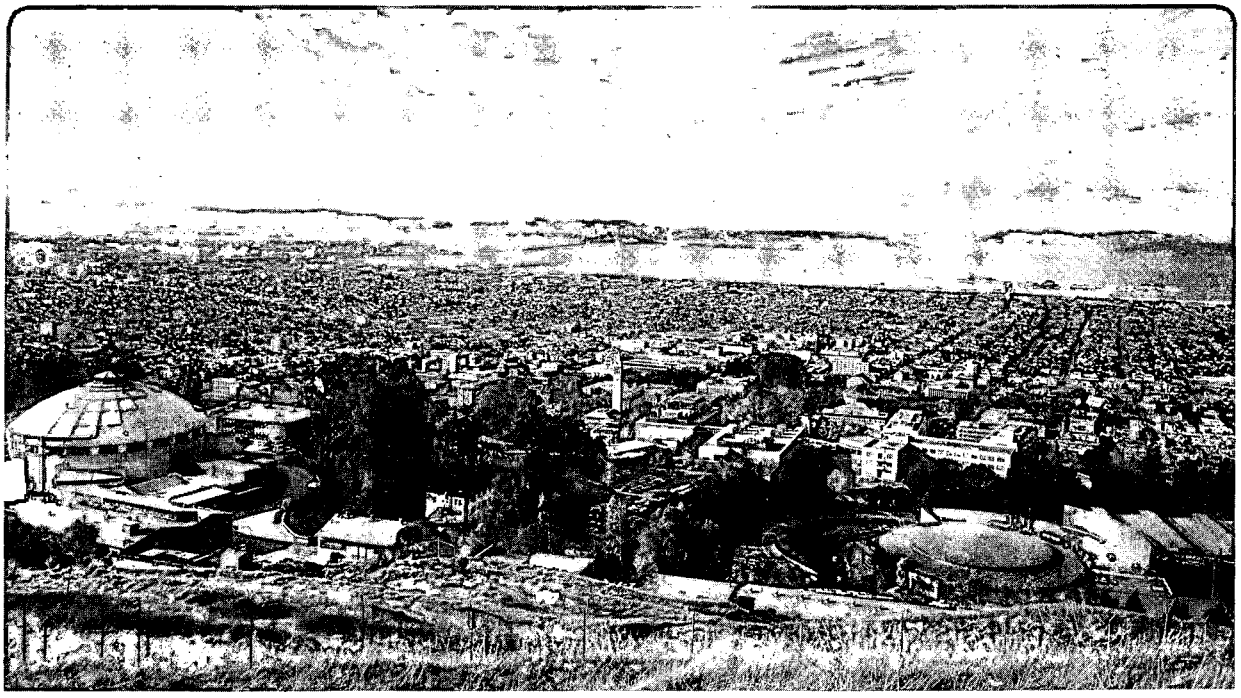

REFERENCE COPY
Does Not
Circulate
Bldg. 50 Library.
LBL-34734
Copy 1

Prepared for the U.S. Department of Energy under Contract Number DE-AC03-76SF00098

DISCLAIMER

This document was prepared as an account of work sponsored by the United States Government. While this document is believed to contain correct information, neither the United States Government nor any agency thereof, nor the Regents of the University of California, nor any of their employees, makes any warranty, express or implied, or assumes any legal responsibility for the accuracy, completeness, or usefulness of any information, apparatus, product, or process disclosed, or represents that its use would not infringe privately owned rights. Reference herein to any specific commercial product, process, or service by its trade name, trademark, manufacturer, or otherwise, does not necessarily constitute or imply its endorsement, recommendation, or favoring by the United States Government or any agency thereof, or the Regents of the University of California. The views and opinions of authors expressed herein do not necessarily state or reflect those of the United States Government or any agency thereof or the Regents of the University of California.

LBL-34734

Crosshole Electromagnetic Imaging for Reservoir Definition and Monitoring

M. J. Wilt,[1] *D. L. Alumbaugh,*[2,3] *H. F. Morrison,*[2,3]
A. Becker,[2,3] *K. H. Lee,*[3] *and M. Deszcz-Pan*[2]

[1]Electronics Engineering Department
Lawrence Livermore National Laboratory
University of California
Livermore, California 94550

[2]Department of Materials Science and Mineral Engineering
University of California

[3]Earth Sciences Division
Lawrence Berkeley Laboratory
University of California
Berkeley, California 94720

July 1993

This work was supported in part by a consortium of energy and service companies, including the research divisions of Arco, Amoco, British Petroleum, Exxon, Shell, Unocal, and Mobil Petroleum Companies, Schlumberger-Doll Research, Zonge Engineering, Noranda Technology, and Nitetsu Mining Corporation, and in part by the Assistant Secretary for Fossil Energy, Office of Oil, Gas and Shale Technologies, under U.S. Department of Energy Contracts W-7405-Eng-48 and DE-AC03-76SF00098.

Abstract

Electrical conductivity is an important reservoir parameter due to its sensitivity to porosity, pore fluid type and saturation. Although it is widely used in borehole logging to obtain the conductivity near boreholes the poor resolution offered by surface-based field electrical and electromagnetic (EM) systems has thus far limited obtaining this information in the region between wells. Low frequency crosshole EM offers the promise of providing subsurface conductivity information at a much higher resolution than was previously possible.

Although the general three-dimensional conductivity inversion problem is too complex for routine use, numerical solutions assuming cylindrical symmetry and low contrast resistivity structure can be used for a large class of reservoir problems. We developed an iterative Born inversion scheme employing cylindrical symmetry and applied it to field data. Field instrumentation was developed using off-the-shelf components when possible but custom-designed induction coil transmitters and receivers were built for the field exercises. The assembled field system has adequate power for moderate to high-resolution imaging using boreholes spaced up to 500 m apart.

The initial field experiment was done in flat lying terrain at the British Petroleum test site in Devine, Texas. Using wells spaced 100 m apart we collected a complete crosshole EM data set encompassing a 30 m thick 10 ohm-m limestone layer at a depth of 600 m. The resulting profiles were repeatable to within one percent and showed an

excellent sensitivity to the layered structure, closely matching the well log. At the UC Richmond field station crosshole EM measurements were made to track an injected slug of salt water. Conductivity images of data collected before and after injection showed a clear anomaly due to the salt water plume and showed that the plume had migrated in a northwesterly direction from the injection borehole.

Introduction

The central problem in petroleum production is the development of a reservoir model that guides the drilling of wells and the management of the field. Ideally the model provides a three-dimensional numerical representation of the petroleum-bearing rock, properties of the reservoir units and the nature of the boundaries. To construct this model the reservoir engineer has only the detailed data from well logs in a limited number of holes, a geologic conceptual model and, more recently, structural controls provided by seismic data. The extrapolation of drill hole data to the interwell volume is a daunting task but it is an area where geophysics can be of great benefit. Using high resolution geophysics to assign physical properties to the model is a relatively new and exciting idea which could revolutionize the effectiveness of reservoir simulation. Papers by Lake (1990), Shelton and Cross (1989), and Savit (1987) eloquently state the need for this.

Seismic velocity and electrical conductivity are both dependent on the porosity, saturation, temperature and anisotropy of typical reservoir rocks and consequently seismic and electrical techniques are a first choice in the search for new reservoir characterization methods. Surface-based 3-D seismic methods have already had a large impact on reservoir engineering by providing detailed maps of the geometry of producing formations and in some cases hydrocarbon distribution (Sherriff, 1992). This is a significant departure from their traditional role of finding target structure in an exploration program.

Electrical conductivity has an even more direct relationship to reservoir fluid properties than do seismic parameters because porosity, pore fluid conductivity, saturation, and temperature all determine the conductivity. Electrical logs are indispensable to the reservoir engineer for assessing saturation, pore fluid type and indirectly, permeability. Electrical logging maps the conductivity in the vicinity of the borehole to a radius of a few meters. Means are now at hand to map the conductivity on a reservoir scale and it is this prospect that motivates this study of cross-borehole electromagnetic methods.

It is instructive to review the relative dependence of seismic velocity and electrical conductivity on reservoir porosity, saturation, and temperature. An empirical, but accurate, formula relating formation resistivity, ρ_f, porosity, ϕ, and pore fluid resistivity porosity, ρ_w ,is given by Archie's Law: $\rho_f = \rho_w \phi^{-2}$. An empirical relationship between velocity, V, and porosity, $\varnothing$, is given by the Wyllie time average relation: $\frac{1}{V} = \frac{\phi}{V_f} + \frac{(1-\phi)}{V_{ma}}$,

where V_{ma} and V_f are the matrix and pore fluid velocities respectively. Using typical velocities for V_{ma} and V_f of 6,000 m/sec and 1500 m/sec respectively and a porosity of 25%, these relations show that a 20% change in porosity results in a formation resistivity change of 40% but a velocity change of only 8%.

Seismic velocities show little sensitivity to partial saturation in oil-water mixtures but the strong dependence of electrical conductivity on saturation is well known from electric logging. The resistivity of a partially saturated rock, ρ_f, is related to the fully saturated formation, ρ_{f0}, by $\rho_f = \rho_{fo} / S_w^2$, where S_w is the pore fraction filled with water. As in the case of porosity, small changes in saturation produce double the effect in formation resistivity. In oil-water and gas-oil mixtures Wang and Nur (1992) show that seismic velocities are essentially independent of S_w until the saturation approaches 100% where the velocity increases dramatically.

The effect of temperature on formation resistivity is also pronounced. As the temperature of an oil-brine saturated rock is raised from 22° to 122°C, the resistivity falls by over 70%. In contrast, Wang and Nur (1992) show decreases in compressional wave velocity in a light hydrocarbon saturated sandstone of 7 to 8% for the same temperature increase and 40% for heavy oil sands.

Although seismic methods are relatively mature, the methodology for measuring electrical conductivity on a reservoir scale is in a developmental stage. Surface low frequency electromagnetic and dc resistivity methods have been applied to process monitoring (Wayland et al. 1982, Wayland et al. 1984, Bartel and Wayland, 1981, Bartel and Ranganayaki, 1990) but they have been limited to identifying the presence and general configuration of relatively shallow processes.High frequency EM (>1MHz) has been used in crosshole configurations since the early eighties (Kretzschmar et al. 1982 ; Laine, 1987) but the low resistivity of most sedimentary formations typically limits the propagation distance of these fields to a few meters (Harben and Pihlman, 1988).

Crosshole and borehole-to-surface configurations typically offer improved sensitivity as compared to surface-based schemes. In surface surveys, the fields must first penetrate, with considerable loss of strength, to the target zone, produce a secondary or scattering current, and the fields from these currents again attenuate greatly in returning to the surface. This attenuation obviously limits the sensitivity of small features at depth. A further complication in surface methods is that the near-surface weathered layer is invariably inhomogeneous and thus exerts a strong attenuation and distortion of the fields from deep targets. Finally, the influence of cultural noise is far greater at the surface than in boreholes.

Getting at least one of the transmitter-receiver pair near the target zone alleviates these problems somewhat (Greaves et al. (1991), Asch and Morrison (1989)) but an even greater improvement occurs if both the source and receiver are placed in boreholes. For example crosshole dc resistivity surveys have far greater resolution than surface or surface-to-borehole configurations (Daily and Owen, 1991).

The work of Zhou (1989) initiated a systematic study of low frequency crosshole EM for reservoir scale problems and showed that a low frequency analog of seismic diffraction tomography provided remarkable resolution of interwell features. In 1989, researchers at LLNL, LBL, and UC Berkeley began a joint program to conduct low frequency crosshole and surface-to-borehole EM measurements and to develop suitable inversion and imaging codes for interpreting field data. The program was designed to develop tools for reservoir characterization and process monitoring.

In this paper we will first review some of the basic theory and discuss several approaches at conductivity imaging of crosswell EM fields. We then describe the equipment that we used for preliminary crosshole measurements, and lastly give results from two field surveys.

Theoretical formulation:

The modeling of crosshole EM data is inherently a difficult proposition. The magnetic or electrical dipole source field has three-dimensional (3-D) characteristics, and in general, so does the medium to be studied. Modeling of electromagnetic fields in a realistic arbitrary 3-D medium is a very complex undertaking, typically exceeding the capabilities of today's supercomputers (Hohmann, 1988). The problem can be cast into somewhat manageable form if the 3-D target is of finite extent and is embedded in a homogenous (or

layered) earth (Newman and Hohmann, 1988). In this case EM fields can be described using integral equations, in which the domain of solution is limited to the area whose conductivity is different from that of the background. This is a useful model for many reservoir features and is particularly useful for operations in which changes in some target volume are to be monitored. Here we give a review of the integral equation formulation.

Maxwell's equations in the frequency domain are written as

$$\nabla \times E = -i\omega\mu H, \tag{1}$$
$$\nabla \times H = (\sigma + i\omega\varepsilon)E + J. \tag{2}$$

where E is the electric field, H is the magnetic field and J represents the electric current source. In the region of interest the conductivity can be written as

$$\sigma = \sigma_b + \Delta\sigma.$$

with the subscript b, designating the conductivity of the background and $\Delta\sigma$, the conductivity perturbation due to the target body. The magnetic permeability is assumed to be uniformly constant everywhere. Equations (1) and (2) can be combined to yield

$$\nabla \times \nabla \times E - k^2 E = -i\omega\mu J, \tag{3}$$

with the propagating constant k defined by

$$k^2 = k_b^2 = \omega^2\mu\varepsilon - i\omega\mu\sigma_b,$$

everywhere in the background and

$$k^2 = k_b^2 + \Delta k^2 = (\omega^2\mu\varepsilon - i\omega\mu\sigma_b) - i\omega\mu\Delta\sigma$$

in the anomalous region. Equation (3) is the wave equation for the electric field. The solution to this equation can be cast as an integral equation employing a Green's function (Hohmann, 1988). For the electric field this has the form

$$E = E_b - i\omega\mu \int \overline{\overline{G}}^J \cdot \Delta\sigma E dv \tag{4}$$

where E_b is the *primary* or *background* electric field that would exist in the absence of any inhomogeneities and $\overline{\overline{G}}^J$ is the 3-D dyadic Green's function which satisfies

$$\nabla \times \nabla \times \overline{\overline{G}}^{J} - K_b^{\,2} \overline{\overline{G}}^{J} = \overline{\overline{I}}\delta . \tag{5}$$

In these equations the superscript J denotes the electric field Green's function and $\overline{\overline{I}}$ is identity matrix. The term $\Delta\sigma E$ inside the integral is called the 'scattering current'; this is the source of the secondary or scattered fields (Harrington, 1961). This current is confined to the anomalous region in which the electrical conductivity is different from the background. Note that we can obtain the magnetic field by taking curl of equation (4),

$$H = H_b + \int \nabla \times \overline{\overline{G}}^{J} \cdot \Delta\sigma E \, dv = H_b + \int \overline{\overline{G}}^{H} \cdot \Delta\sigma E \, dv . \tag{6}$$

where the superscript H now denotes the magnetic field Green's function.

Equations (4) and (6) are 3-D integral equations of the second kind. They are nonlinear due to the appearance of the unknown electric and magnetic fields both inside and outside of the integrals. Rigorous solution of these equations typically involves considerable computational time and is complicated by numerical instabilities, such as the singular cell calculation. Because of these difficulties, direct inversion for the conductivity distribution is presently not feasible except for simple problems.

If the scattering region is electrically small, (i.e. its field does not perturb the background field) then the problem can be linearized and simplified by applying the Born approximation (Kong, 1975). This is a simple process of substituting the background electric field for the total electric field in the integral. For this to be valid the frequency-conductivity volume product of the scatterer must be small enough so that the scattered field is small compared to the background field. When this is applied equation (4) becomes

$$E = E_b - i\omega\mu \int \overline{\overline{G}}^{J} \cdot \Delta\sigma E_b dv , \tag{7}$$

while the approximate magnetic fields have the form

$$H = H_b + \int \nabla \times \overline{\overline{G}}^{J} \cdot \Delta\sigma E_b dv . \tag{8}$$

These equations are known as the 'zero order' Born approximations for the electric and magnetic fields.

Even with this useful approximation, inverting crosswell EM data for a 3-D conductivity distribution is still difficult. Not only are an inordinate amount of data

required, but the size of the problem soon becomes too large for all but the largest computers to handle. Fortunately, for a large class of problems a more simplified geometry can be applied. For example, although the field-wide resisitivity changes associated with an enhanced oil recovery (EOR) operation are three-dimensional, the resistivity changes around a single injector may be approximated by a two-dimensional model with cylindrical symmetry (Figure 1). By collecting crosshole EM data in several planes around an injection well (or a nearby temperature observation well) it is reasonable to approximately reconstruct the resistivity distribution around the well during steam injection and thereby infer flow paths for the steam. Since both the resistivity changes due to the fluid injection and the volume of formation affected are quite large there is a reasonable expectation that employing such a geometry would provide a good results. As a starting point for more general inversions we have assumed this cylindrical symmetry for interpreting field data.

When the cylindrically symmetric geometry is employed, the tensor integral equations given in equations (4) through (8) reduce to a scalar form. Thus equations (7) and (8) for the Born approximation take the form

$$H = H_b + \int \Delta\sigma E_b G^h da \tag{9}$$

for the magnetic field and

$$E = E_b + \int \Delta\sigma E_b G^j da \tag{10}$$

for the electric field. Here the lower cased superscripts on the Green's functions symbolically designate scalar rather than dyadic functionals and the integration is carried out over a cross sectional area between the wells rather than a 3-D volume.

Following the work of Wu and Toksoz (1987), Zhou (1989) developed a solution to equation (9) in the *wave-number* domain rather than in the space domain and he called this method *electromagnetic diffusion tomography*. However, because the earth often includes large high contrast anomalies, the zeroth order Born approximation as employed by Zhou (1989) is sometimes ineffective.

A more rigorous approach of imaging the conductivity structure uses an *iterative Born inversion* scheme (Alumbaugh and Morrison, 1992). In this approach, an initial image of the anomalous conductivity is reconstructed using the zeroth order approximation by inverting for $\Delta\sigma$ in equation (9). The total electric field inside this anomalous

distribution is then calculated using forward modeling. The total electric field is then substituted for E_b in equation (9) and a new estimate of $\Delta\sigma$ obtained. The forward modeling and inversion steps are then repeated iteratively until convergence occurs. We found this approach to work well in the examples described below.

Design of a Cross-Borehole EM System

In this section we describe the criteria for designing a crosshole EM system, making use of simple models to determine the optimum transmitter power (dipole moment), receiver sensitivity and the operating frequencies. Other design considerations include allowable dimensions (i.e. to deploy in boreholes), weight and durability.

Spies and Habashy (1992) and Alumbaugh and Morrison (1992) show that the kernel inside the integral of the zeroth order Born approximation when multiplied by $\Delta\sigma / \sigma_b$ can be used to define the sensitivity of a given source receiver pair to the region between the wells. This sensitivity function is known as the Frechet derivative and has the form

$$K_{Hz} = \sigma_b G^{hz} E_{\phi b} \tag{11}$$

Figure 2 shows the amplitude of K_{Hz} assuming a cylindrical geometry for a point centered between a source and receiver at the same depth. The kernel is plotted as a function of the background induction number ($\omega\mu\sigma_b R^2$) to allow us to determine the sensitivity for a range of frequency-conductivity-interwell spacings. The scattered field for an electrically small body is proportional to this sensitivity function. The abscissa of this graph starts at an induction number of 0.01 and terminates at 1000. Below 0.01 the total field is almost equal to that of the free space value (Spies, 1992), above 1000 the fields are difficult to measure due to attenuation.

Several important characteristics about crosswell EM can be derived from this diagram. At induction numbers less than 1.0 the scattered field is small, indicating that the response of small or poor conductors will be difficult to measure. The kernel amplitude is maximum at induction numbers from 5 to 100. This corresponds to 2 to 10 plane-wave skin depths, where the skin depth is defined as the distance a plane wave attenuates to 1/e its initial value and is given by $\delta = \sqrt{\frac{2}{\sigma\omega\mu}}$. This represents the region in which the

scattered fields will be most easily detected and it can be used as a rule of thumb when designing surveys. For induction numbers above 100 both the kernel and the primary field fall off rapidly due to attenuation.

We can readily obtain a minimum value of transmitter moment required by noting that for coplanar vertical magnetic dipole transmitters and receivers in a conductive whole space the magnetic field is given by:

$$H_z = \frac{-M}{4\pi r^3} e^{-ik_b r} (1 + ik_b r - k_b^2 r) \qquad (12)$$

(Kauffman and Keller, 1983). Here, M, is the transmitter dipole moment, r, is the interwell distance and k_b is the propagation constant of the background medium as defined previously. If we neglect the displacement currents, then the vertical magnetic field in this geometry is a function of conductivity-frequency product and separation only. In Figure 3 we plot the vertical magnetic field amplitude for coplanar transmitter-receiver pairs. The plot gives the field for a range of well separations, frequencies and conductivities using transmitter moment of 1; it also shows the "noise floor "assuming that the noise is equal to the maximum sensitivity of our existing receiver, or 10^{-7} nT. Note that by increasing the transmitter moment the noise floor moves downward proportionately. For example if a transmitter moment of 10^3A-m^2 is used the noise floor moves from 10^{-7} to 10^{-10} nT. Figure 3 shows that the field displays $1/r^3$ field fall of characteristic of free-space EM fields up to a $\sigma f r^2 = 4\text{x}10^6$, above this the attenuation is exponential. This corresponds to the background induction number of 30, or approximately 20 skin depths.

The plot gives a range of investigation for crosshole EM. For example assuming a background conductivity of 0.1 S/m and a source moment of 1000 the figure shows that we can do effective crosshole imaging at borehole separations from 10 to more than 1000 m. At a well separation of 100 m and a background conductivity of 0.1 S/m the plot indicates that frequencies in the range from 1000-100,000 Hz can be used for imaging.

LLNL/LBL Crosshole EM System

Using the above design criteria we assembled and tested crosshole EM systems for two field trials. The deep test in Devine, Texas used wells 100 m apart and several km deep; the shallow test at Richmond, California used wells less than 50 m apart and 100 m

deep. In practice the two field systems were identical except for the transmitter tool and associated winch.

The measurement system is modular. It consists of a transmitter section that includes a transmitter solenoid, a current source to drive it, and a winch and cable system for downhole deployment of the source. The receiver module consists of a commercial sensor attached to an armored cable, one stage of surface amplification and filtering and a commercial synchronous detector, which uses the optically coupled transmitter current signal as a reference; data is logged using a desktop computer.

Transmitter and receiver modules for this system are essentially separate entities. That is, the receiver may be used with separate transmitters, and several separate receivers could be operated using the same transmitter. The modules are connected only via electrically isolated cables. Instrumentation from each module is required to be locally grounded, have its own power supply and be electrically isolated from other modules. Such grounding and isolation is vital for the elimination of stray currents and ground loops that degrade data quality.

Transmitter Section:

A schematic diagram of our crosshole transmitter system is given in Figure 4. Although a downhole oscillator is preferred, simplicity of assembly dictated that the initial transmitter be powered from the surface. We built our first transmitter around a laminated magnetic steel (mu-metal) core previously used on an airborne EM system (the McPhar F-400). This core was chosen because of its availability and the relatively low frequency (100-4,000 Hz) required for the Devine test. It is 2.4 m long and 7.5 cm in diameter and when wound uniformly with 350 turns of wire this solenoid has an effective relative magnetic permeability of about 150 and an inductance of about 40 mH; a moment of 1000 A-m^2 is readily achieved with a current of 5A.

The maximum moment is limited by the current and the number of turns required to saturate the core with magnetic field (Holladay and Wilt, 1993).This, in turn, is typically determined by the volume and type of core material. For this particular mu-metal core the maximum moment is approximately 10,000 A-m^2. The associated inductive reactance is canceled by series tuning the solenoid with an appropriate capacitor located in the solenoid casing. Core losses rise very sharply with frequency due to hysterisis effects and eddy

currents induced in the conductive steel core. About 1 kW of power is required to drive the solenoid with 5A when the frequency is raised to 1 kHz. Above 5 kHz the output is reduced to unacceptable levels.

Because of the higher projected operating frequency at the Richmond test site we elected to use a ferrite core for the transmitter solenoid. Ferrite is the preferred material at high frequencies because it is essentially nonconductive and therefore not suseptible to eddy current losses. Making use of readily available material we constructed a tubular core made up of a large number of stacked 1.27 cm thick ferrite (Sprang model P44416-TC) toroids. The resulting tube has an outside diameter of 4.4 cm and a length of 197 cm. The diameter of the inner void space was 1.91 cm. The core was wound with 125 turns to maximize the output at 18 kHz and had an inductance of about 2 mH. This resulted in a moment of about 100 A-m^2 using a current of 3.5 A . The effective relative magnetic permeability for this core was also about 150. The core losses were much lower so that only about 125 W of power were needed to drive the resonant transmitter circuit.

Due to the different power requirements at the two test sites the transmitter solenoids were driven by different current sources in each case. At the Devine site we used a Zonge GGT-20 transmitter driver. Although this device generates a square waveform it is filtered by the resonant transmitter circuit so that the resultant transmitted signal very nearly resembles a sine wave at the fundamental frequency. At the Richmond test site the power requirements were much lower and could be easily met by using an ordinary laboratory signal generator coupled to a Crown model 610 power amplifier with an output of 600 W.

The large transmitter coil and cable are moved with a hydraulic, diesel powered winch which advances the tool at a steady rate ranging from several to several hundred meters per minute. The cable drum can hold about 1500 m of seven conductor logging cable. We use a lightweight portable electrical winch, that holds 200 m of cable, to move the smaller ferrite coil. This lightweight winch and coil may be easily moved by two people and are convenient to use in shallow applications. For each tool the transmitter depth and rate of movement are monitored with a wheel-driven encoder/counter. In addition to providing depth information this encoder pulse also serves as a data acquisition trigger at the receiver.

The transmitter current is detected with an inductive-type current meter connected to the source output. This analog record of the current is sent to the receiver via an isolated

line where it is used as a phase reference. Note that the current is only roughly proportional to the source moment due to the non linearity of the core material. We therefore rely on calibration corrections to determine the source moment from the transmitter current measurement. A second isolated line provides an analog record of the encoder pulse.

Receiver Section:

Signals are detected at the receiver using a vertical-axis custom-designed borehole coil (Electromagnetic Instruments Inc., model number BF8DH). This receiver coil is an ultrasensitive device (maximum sensitivity of 10^{-13} teslas (T)), operable in the frequency range from 1-100,000 Hz. The tool is housed in a pressure vessel designed for depths up to 2 km. Detected signals are amplified within the coil then transmitted to the surface up the logging cable. At the surface they are further amplified and filtered before input to the receiver van (Figure 6). In the van all instruments are controlled from a desktop computer via the GPIB interface. The computer can adjust instrument gains and sensitivities as well as select sample and averaging rates for the logging system.

Note that while the tool sensitivity is rated at 10^{-13} T the maximum sensitivity we have achieved is approximately 10^{-11} T. This disparity is likely due to incomplete source-receiver isolation and the effects of external noise.

Data logging at the receiver is triggered by encoder pulses originating at the transmitter.The computer counts the incoming pulses until one corresponding to a pre-selected measurement depth is received. The computer then collects transmitter current data from the digital voltmeter and magnetic field data from the lock-in detector. The lock-in detector uses the transmitter current wave form as a reference signal and detects receiver signals in-phase and out-of-phase. It is a very effective device for accurately discriminating low level signals in a noisy background. The spectrum analyzer depicted in Figure 5 is used for debugging and calibrating system components.

Cross-Borehole Logging :

A particular borehole segment is logged by moving the transmitter coil upwards at a fixed rate while the receiver remains stationary in another borehole. Although equivalent information could be collected by moving the receiver coil while the transmitter is fixed, doing so results in very noisy data due to the motion of the sensitive detector in the earth's

magnetic field. The source coil is typically moved at a rate of 3-5 m /minute. This allows sufficient time for signal averaging but is still a reasonable rate for data collection.

Data is collected in one-half to one meter intervals within a logging span; at each measurement point five readings are averaged as the transmitter moves past. We typically log over a depth interval that is 1.5-2.0 times longer than the separation between boreholes; this is a minimum interval required for tomographic reconstruction (Zhou, 1989). Ten to fifteen receiver stations are usually spaced to cover the depth interval traversed by the transmitter.

Field Test 1: British Petroleum Test Site Devine, Texas

The Devine test site, established by British Petroleum to test geophysical methods and instrumentation, is located some 50 km southwest of San Antonio, Texas (Figure 6). It is situated in an isolated area, away from sources of cultural noise, but still within reasonable access to population centers. Three boreholes are available for experimental use; boreholes #2 and #4 are 100 m apart; they are steel-cased to 160 m and plastic lined below this to a depth of 900 m. Borehole #9 is steel-cased to a total depth of 900 m. The geology at the site consists of a sequence of sandstones, shales and limestones. Individual beds are continuous and flatlying across the entire site as is evident from an examination of the well logs. The borehole resistivity logs show variations from 1 to 300 ohm-meters with the higher resistivity layers (limestones) concentrated towards the base of the section and the sandstone and shale layers ranging in resistivity from 1 to 10 ohm-m .

We chose to collect a set of crosshole profiles that span a 120 m depth section from 550-670 m. This segment includes 2-3 ohm-meter sands and shales and a 30 m thick 3-10 ohm-m predominantly limestone strata and back to sands and shales (see Figure 7). For each profile the source moves between fixed depths 120m apart and the receiver remains fixed in the other borehole at a depth within these limits. Subsequent profiles are then made between the same source positions using different receiver locations. A set of profiles corresponds to 13 receiver position, spaced 8 m apart, covering a similar depth span as the source coil.

Sample crosshole magnetic field plots are given in Figure 8. The plots show the amplitude and phase of the vertical magnetic field at a frequency of 512 Hz as the transmitter moves between 550 m and 670 m in one borehole while the receiver is fixed at a

depth of 598 m in a second borehole 100 m away. The magnetic field amplitude, given in picoteslas (pT) per unit dipole moment, is a smooth curve that forms a peak where the source and receiver coils are in closest proximity and an approximately symmetrical decrease in field strength away from the peak. The transmitter moment is approximately 1000 A-m^2 so the detected fields are in tens of pT. The phase data are also smooth but they display more character than the amplitudes. Near a depth of 600 m the phase forms a peak and it "rolls off" sharply above this. This sharp phase rotation correlates with a decrease in subsurface resistivity as the transmitter passes from resistive limestone below 600 m to less resistive sands and shales above this depth.

The above profile was measured twice on successive days to establish the precision of the system; the difference between the data sets is displayed in Figure 9. This figure shows the amplitude difference over the 24 hour period to be less than 1.0 percent for all points with an average of 0.3 percent. The phase difference averaged less than 0.2 degree. Both of these are well within the guidelines of 1.0 percent for amplitude variations and 0.5 degrees for phase established for imaging requirements (Zhou, 1989). Reciprocity measurements were done in these same boreholes by interchanging the source and receiver tools. These measurements also agree to within one percent but the differences are about twice as high as the repeated data shown above.

The crosshole amplitude and phase data for the above profiles using a frequency of 512 Hz are shown as contour plots in Figure 10. Each contour plot consists of a series of amplitude (or phase) profiles, one for each receiver, contoured to form a continuous plot. The amplitude data dominantly reflect the relative positions of the source and receiver coils, peaking where the coils are in closest proximity. The peak amplitudes are larger in the lower parts of the section which corresponds to a zone of higher resistivity, (and lower field attenuation). In contrast, the phase data are rich in character showing a smooth, continuous variation of more than 60 degrees within the depth span. The maximum phase values generally correspond to the high resistivity limestone, the minimum phases correspond to the lower resistivity sands and shales. The contact between these layers, located at a depth of 600 m, can be correlated with sharp gradients in the phase.

We initially interpreted the Devine EM data using a layered model inversion. The code was developed by two of the authors (Deszcz-Pan and Lee) using an inversion technique given by Anderson (1982). In general, the layered inversions were very well behaved and the resulting models derived from inverting individual profiles compare

closely. This is in large part due to the simple stratified geology at the Devine site. In Figure 11 we show a comparison of the layered model inversion for the profile from receiver station 609.75 to the borehole induction log spanning the same depth interval. The resisitivity values from the inverted section and the induction log are remarkably close.

Figure 12a shows a conductivity image derived from the 512 Hz Devine data using the iterative Born inversion described above. It is plotted with a smoothed version of the well log given in Figure 7. The image indicates primarily one-dimensional geometry with a resistive zone, corresponding to the limestone layer, extending from approximately 600m to 630m in depth. The correlation between the well log and the tomogram is remarkably good especially near the receiver well. The image also indicates a considerable amount of two-dimensional structure. The resistive layer is shown to be thicker near the receiver well while the regions above and below this are more conductive near the source well.

In order to determine if these 2D artifacts are a function of the inversion algorithm or the data, we calculated a synthetic data set for a layered model using the 1D inversion results and the same source-receiver geometries. The inversion of these calculated results (Figure 12b) show similar 2D artifacts although not as extreme. The fact that the 2-D effects are less pronounced in Figure 12b is possibly due to small amounts of systematic drift in the Devine data. Alumbaugh (1993) has shown that the imaging scheme is extremely sensitive to this type of correlated noise. However, the artifacts can also partially be explained by a lack of vertical coverage in the survey. To demonstrate this effect a model was calculated which extended the array 40m upward from 550m to 510m. As Figure 12c indicates the added vertical coverage improves the horizontal resolution. All layers except the resistive zone at 560m are now shown to extend continuously across the region.

Field Test 2: Saltwater Injection Monitoring at UC Richmond Field Station

The Richmond test facility lies approximately 12 km north of the UC Berkeley campus and adjacent to the San Fransisco Bay (Figure 13). From April to August, 1992 we used this facility to inject a slug of salt water and monitor its emplacement and movement with crosshole EM. The experiment consisted of injecting 250,000 liters of 1.ohm-m saltwater into a 3 m thick aquifer at a depth of 30 m through a perforated zone in well INJ1 and collecting EM data before and after injection.

Figure 14 shows borehole induction logs from wells EMSW and EMNE together with stratigraphic logs made from well cuttings. The upper 30-35 m at Richmond field station consists of discontinuous unconsolidated muds, silts and variably thick layers of sand and gravel with resistivities ranging from 5 to 30 ohm-m. Below the unconsolidated sediments is a basement consisting of sandstone or shale, most likely from the Cenozoic Great Valley formation. The sandstone basement encountered beneath boreholes INJ, INJ1, EMSE, EMSW and EMNW has a resistivity of 100 ohm-m or more; the shale found beneath EMNE has a resistivity of 40-60 ohm-m. A description of the site geology is provided in Pouch (1987) who found that only a few of the water-bearing sands and gravels, could be traced across the field and that these varied considerably in thickness.

The crosshole EM measurements were made using a five well set with the transmitter deployed in the central borehole (INJ1) and the other boreholes (EMNE, EMNW, EMSE and EMSW) used for the receiver tool. This arrangement provides the first-order cylindrical symmetry required by our present imaging code (Alumbaugh and Morrison, 1992). The EM data were collected at a frequency of 18.5 kHz using the small transmitter and portable winch. Profiles were collected using receivers spaced at 5 m intervals from the surface to a depth of 60 m and a continuously moving transmitter with data collected each 0.5 m. A total of ten sets of crosshole data were collected, four before and six after injection. We also collected induction resistivity logs and measured water conductivity in all holes before and after salt water injection.

To ensure that the system was operating properly transmitter profiles were repeated at the beginning of each day and whenever the receiver was moved to a new well. In general an average of 2% amplitude error and 1° phase difference were considered good stability bounds for the system. Due to time considerations however, we sometimes accepted greater amplitude errors if the phase was stable and vice versa. Extra sets of post-injection data were collected in the EMNW and EMSW wells 5 days and 2 weeks after the original data, respectively for error and noise analysis.

The overall mean error and standard deviation between the original and repeat measurements are presented are in percent amplitude and degrees phase in Table 1. The table shows that both the mean error and standard deviation are greater for the EMSW repeat surveys compared to those done in the EMNW well. These larger errors may be due in part to the greater distances between INJ1 and EMSW, and the larger time separation between repeats.

Table 1: Error analysis for EMNW and EMSW wells

	E M N W		E M S W	
	% Amp.	Degrees Phase	% Amp.	Degrees Phase
Mean Error	2.26	-0.81	3.30	-1.09
Standard Deviation	1.40	0.92	2.18	1.31

In Figure 15 we examine two induction logs from borehole INJ1, the salt water injection well. One of these logs was collected before salt water injection and the other after; the difference between them indicates the change in resistivity around the injection well due to the salt water. The logs show that from a depth of 23 to 31 m the resistivity has decreased due to the salt water injection. In the injection interval the two logs are a mirror image, where the higher resistivity sands and gravels before the injection have become the lower resistivity units after the salt water injection. The largest decrease is observed in a 4 m thick sandy-gravel aquifer at a depth of 26-30 m where the well is perforated. The rock in this interval has decreased in resistivity from 15 ohm-m to 3.5 ohm-m. Using a dirty sand model (Waxman and Thomas, 1974) we predicted that the salt water should change the formation resistivity to 3 ohm-m. These calculations were done assuming a rock porosity of 25 percent, clay content of 20 percent and salt water conductivity of 1 S/m.

Crosshole EM amplitude and phase measurements collected before and after saltwater injection appear only subtly different due to the saltwater; the effects of the injection become apparent if we calculate the secondary fields resulting from the introduction of the plume. This is a simple process involving the subtraction of the fields measured before the injection from those measured after injection.

We show the resulting anomalies for wells EMNW and EMSW in Figures 16 and 17. Figure 16 clearly indicates large changes especially around the injection depth whereas the secondary fields in EMSW appear noisier and show a smaller and markedly different anomaly in the injection zone. Secondary fields in EMNE and EMSE are intermediate between the cases shown above. This behavior suggests that the saltwater plume is moving away from INJ1 in a northerly direction rather than spreading symmetrically about the injection well. It is also consistent with earlier dc resistivity experiments (Bevc and Morrison, 1991).

We interpreted the crosshole EM data at Richmond by inverting the pre and post injection profiles for each well separately. This was necessary because the irregular geology and resistive basement meant that we could not restrict our image to the injection zone. Thus rather than inverting only for conductivity changes resulting from the injection, the entire conductivity structure between the two wells was imaged both before and after injection. The background conductivity used in the inversion was chosen by minimizing the magnitude of the secondary field.

Conductivity images for EMNW before and after injection are plotted in Figures 18a and b. The pre-injection image shown in Figure 18a shows a conductive overburden overlying a more resistive basement. This is consistent with the borehole induction logs. The post-injection image (Figure 18b) clearly shows a region of high conductivity at 30m depth near the source well that is not present prior to injection. This anomaly corresponds to the injection zone and strongly suggests that salt water has migrated to the northwest. This agrees with the results published by Bevc and Morrison (1991). Images of the EMNE data indicate some migration to the northeast while the EMSW and EMSE results indicate almost no migration to the southeast or southwest.

The direction of plume migration becomes more apparent if we plot the change in conductivity between the before and after images. This is a simple process of subtracting the conductivities in the pre-injection image from those in the post-injection image on a cell by cell basis. As Figure 19 shows, large changes in conductivity occur between INJ1 and both of the northern wells. The fact that the magnitude of the changes in the EMNW well is slightly greater than those in the EMNE well suggests that the water might be moving preferentially in this direction. To the south the changes are much smaller in magnitude and are in negative rather than positive. This implies that little of the injected water is migrating in this direction.

A more careful inspection of the images in Figures 18 and 19 shows some structures that are not consistent with the known geology. Figure 18a indicates that the interface between the conductive sediments and the basement is dipping to the northwest. Although the Richmond geology is fairly complex, the well logs plotted on each side of the images clearly show that the contact is flat. Other errors appear in the difference images (Figure 19). The conductivity changes in the EMNW and EMNE images indicate that the injection causes the sediments near the receiver wells and just beyond the plume boundaries

to become more resistive. To the south these images indicate resistive anomalies near the injection zone and conductive anomalies near the receiver.

Alumbaugh (1993) has determined that these artifacts are due to the cylindrical symmetry employed in the iterative Born imaging scheme. For background induction numbers above 10 a given source and receiver pair is sensitive to the region immediately between them. At induction numbers lower than this the array senses large areas outside of the interwell region and thus the fields generated by a given source-receiver pair contain three dimensional effects which are not accounted for by the 2-D cylindrical symmetry . These 3-D effects can produce images that are not representative of the conductivity structure between the wells. Because the Richmond field station data incorporate an induction number of approximately 4, the artifacts present in these images are probably the result of the three dimensional nature of the subsurface conductivity distribution. To avoid these types of problems, higher frequencies can be employed, or the imaging scheme should be developed assuming a 2 1/2D or 3-D geometry.

Although the tomograms of the Richmond data are flawed due to three dimensional artifacts, they do offer approximate images that are roughly representative of the electrical structure. In addition, the differences of the pre and post injection images correctly identify the direction of greatest fluid migration which will be extremely useful in mapping EOR processes. These results can also serve as a starting model for a more rigorous 3-D inversion such as that employed by Newman (1992). These tomograms may thus be considered as the second step in a three or four step process to interpret the subsurface conductivity structure.

Discussion and Conclusions

The examples displayed above show that moderate to high resolution conductivity imaging is possible with crosshole EM induction. Although there are a number of petroleum and environmental applications that can benefit from this resolution now, the method is still in its infancy and higher data quality and higher resolution imaging will be achieved in the future.

In the near term we can expect significant advances in both hardware and software. Single frequency downhole oscillators are presently under development and a multi-frequency transmitter is not too far behind. Several groups are working on a borehole

transient systems although these are by nature more difficult. Imaging software is under development at several research labs; many of these newer codes are designed to handle the high contrast anomalies and make use of multi-frequency or transient data.

Operating in steel-cased wells is a fact of life in many oil fields. The steel casing effectively limits the operating frequency to a few hundred Hz and thereby reduces the potential resolution of conductivity images. It is possible to collect useful data if wells are widely spaced, thereby requiring low frequencies, or if a surface transmitter can be used.

Acknowledgments

Funding for this research was provided in part by a consortium of energy and service companies, including the research divisions of Arco, Amoco, British Petroleum, Exxon, Shell, Unocal, and Mobil Petroleum Companies, Schlumberger-Doll Research, Zonge Engineering, Noranda Technology, and Nitetsu Mining Corporation, and in part by the Assistant Secretary for Fossil Energy, Office of Oil, Gas and Shale Technologies, under U.S. Department of Energy Contracts W-7405-Eng-48 and DE-AC03-76SF00098.

We would like to thank field technicians Don Lippert, Ray Solbau from LBL's Geophysical Measurement Facility and Louis Preciado on behalf of British Petroleum for their contributions to the data collection at Devine, and Ocean Tseng and Jim Dougherty for their contributions at Richmond field station.

References

Alumbaugh, D.L., 1993, Iterative Electromagnetic Born Inversion Applied to Earth Conductivity imaging., Ph.D. thesis Univ. of California, Berkeley.

Alumbaugh, D.L., and Morrison, H.F., 1992, Tomographic imaging of crosshole EM data: 62nd Ann. Internat. Mtg., Soc. Expl. Geophys., Expanded Abstracts, 495-497.

Anderson, W.L., 1982., Adaptive nonlinear least - squares solution for constrained or unconstrained minimization problems (Subprogram NLSOL): U.S. Department of Interior Geological Survey, Open-File Report, 82-68.

Asch, T.H., and Morrison, H.F., 1989, Mapping and monitoring electrical resistivity with surface and subsurface electrode arrays: Geophysics, **54**, 235-244.

Bartel, L.C., and Ranganayaki, R.P., 1990, Acquisition of controlled-source audiofrequency magnetotelluric (CSAMT) data at an active steam drive site: 59th Ann. Internat. Mtg., Soc. Expl. Geophys., Expanded Abstracts, 213-218.

Bartel, L. C., and Wayland, J.R., 1981, Results from using CSAMT geophysical technique to map oil recovery processes: Soc. Petrol. Eng., Paper SPE 11192.

Beasley, C.W., and Ward, S.H., 1986, Three-dimensional mise-a-la-masse modeling applied to mapping fracture zones: Geophysics, **51**, 98-113.

Bevc, D., and Morrison, H.F., 1991, Borehole-to-surface electrical resistivity monitoring of a salt water injection experiment: Geophysics, **56**, 769-777.

Daily, W.D., and Owen, E. ,1991, Cross-borehole resistivity tomography: Geophysics, **56**, 1228-1235.

Greaves, R.J., Beydoun, W.B., and Spies, B.R., 1991, New dimensions in geophysics for reservoir monitoring: SPE Formation Evaluation, Paper SPE 20170, 141-150.

Habashy, T.M., Groom, R. W.,and Spies, B.R., 1993, Beyond the Born and Rytov approximations: a nonlinear approach to electromagnetic scattering: Journal of Geophys. Research, **98**, no. B2, 1759-1775.

Harben, P., and Pihlman, M., 1988, Thermal front tracking with cross-borehole electromagnetic imaging: Proceedings from Supporting Technology for Enhanced Oil Recovery: EOR Thermal Processes. Department of Energy report DOE/BC-89/1 SP.

Harrington, R. F., 1961, Time-harmonic electromagnetic fields: McGraw-Hill Book Co.

Hohmann, G., 1988, Numerical modeling of electromagnetic fields: *in* Nabighian, M., Ed., "Electromagnetic theory in Applied Geophysics", Society of Exploration Geophysicists.

Holladay, G., and Wilt, M.J., 1992, Design and fabrication of a low frequency induction coil transmitter: report for U.S. Department of Energy report (in press).

Kretzschmar, J.L., Kibbe, K.L., and Witterholt, E.J., 1982, Tomographic reconstruction techniques for reservoir monitoring, Presented at the 57th Annual Fall Conference and Exhibition of the SPE and AIME, Paper SPE 10990.

Kong, J. A., 1975, Theory of Electromagnetic Waves: John-Wiley & Sons.

Laine, E.F., 1987, Remote monitoring of the steam-flood enhanced oil recovery process: Geophysics, **52**, 1457-1465.

Lake, L.W., 1990, What engineers need for numerical simulation, Univ. of Ariz. and Soc. Expl. Geophys. International Symposium on Borehole Geophysics: Petroleum, Hydrogeology, Mining and Engineering Applications, Feb. 1990.

Newman, G.A., and Hohmann, G.W., 1988, Transient electromagnetic responses of high-contrast prisms is a layered earth: Geophysics, **53**, 691-706.

Newman, G. A., 1992, Three-dimensional electromagnetic inversion of insufficient and inadequate data: 62nd Ann. Internat. Mtg., Soc. Expl. Geophys., Expanded Abstracts, 453-456.

Pouch, G.W., 1987, Hydrogeological site assessment of the Engineering Geoscience Well Field at the Richmond Field Station, Contra Costa County, California. M.Sc. thesis, Univ. of California, Berkeley.

Savit, C., 1990, Geophysics and computers: A look to the future: The Leading Edge, **9**, 21-23.

Savit, C., 1987, New ways to study the earth, *in* Research needs for hydrocarbon fuels, Workshop Report on not yet visible or recoverable hydrocarbons, May 11-13, 1987, Houston Area Res. Ctr., U.S. Department of Energy, Office of Basic Energy Sciences, CONF-8705179m, 16-18.

Sena, A. G., and Toksoz, M., 1990, Simultaneous reconstruction of permittivity and conductivity for cross hole geometries: Geophysics, **55**, 1302-1311.

Shelton, J.L., and Cross, T.A., 1989, The influence of stratigraphy in reservoir simulation, *in* Cross, T.A., Ed., Quantitative dynamic stratigraphy, Prentice Hall, 589-600.

Sherriff, R. E., 1992, Basic petrophysics and geophysics, *in* Sheriff, R.E., Ed., Reservoir Geophysics: Society of Exploration Geophysics, 37-50.

Shima, H., 1990, 2-D and 3-D resistivity image reconstruction by combined use of alpha centers and finite elements: 60th Ann. Internat. Mtg., Soc. Expl. Geophys., Expanded Abstracts, 554-557.

Spies, B.R., 1992, Survey design for cross-well electromagnetics: 62nd An Internat. Mtg., Soc. Expl. Geophys., Expanded Abstracts, 498-501.

Spies B.R., and Habashy, T., 1992, Sensitivity analysis of cross-well electromagnetics. 62nd. Internat. Mtg., Soc. Expl. Geophys, Expanded Abstracts, 502-505.

Waxman, M.H., and Thomas, E.C., 1974, Electrical conductivities in shaly sands -1.The relation between hydrocarbon saturation and resistivity index -II. The temperature coefficient of electrical conductivity: Journal of Petroleum Technology, 213-225, Transactions AIME, 257.

Wayland, J.R., Lee, D.O., Montoya, P.C., and Marshall, B.W., 1982, Controlled source audio-magnetotellurics (CDAMT) resistivity measurements for in situ combustion: DOE-Contractor Annual Report Meeting, San Francisco, July 27-29.

Wayland, J.R., Lee, D.O., and Cabe, T.J., 1984, Mapping of a steamflood in a Utah tar sand by controlled source magnetotelluric survey: SPE/DOE 12675, SPE/DOE 4th Symp. on Enhanced Oil Recovery, Tulsa, OK, April 15-18.

Wang, and Nur, 1992, Aspects of rock physics in seismic reservoir surveilance: *in* Sheriff, R.E., Ed., Reservoir Geophysics, Society of Expl. Geophys., 285-300.

Wu, R. S., and Toksoz, M. N., 1987, Diffraction tomography and multisource holography applied to seismic imaging: Geopysics, **52**, 11-25.

Zhou Q., 1989, Audio frequency numerical modeling and tomographic inversion for reservoir evaluation: Ph.D. thesis, Univ. of California, Berkeley.

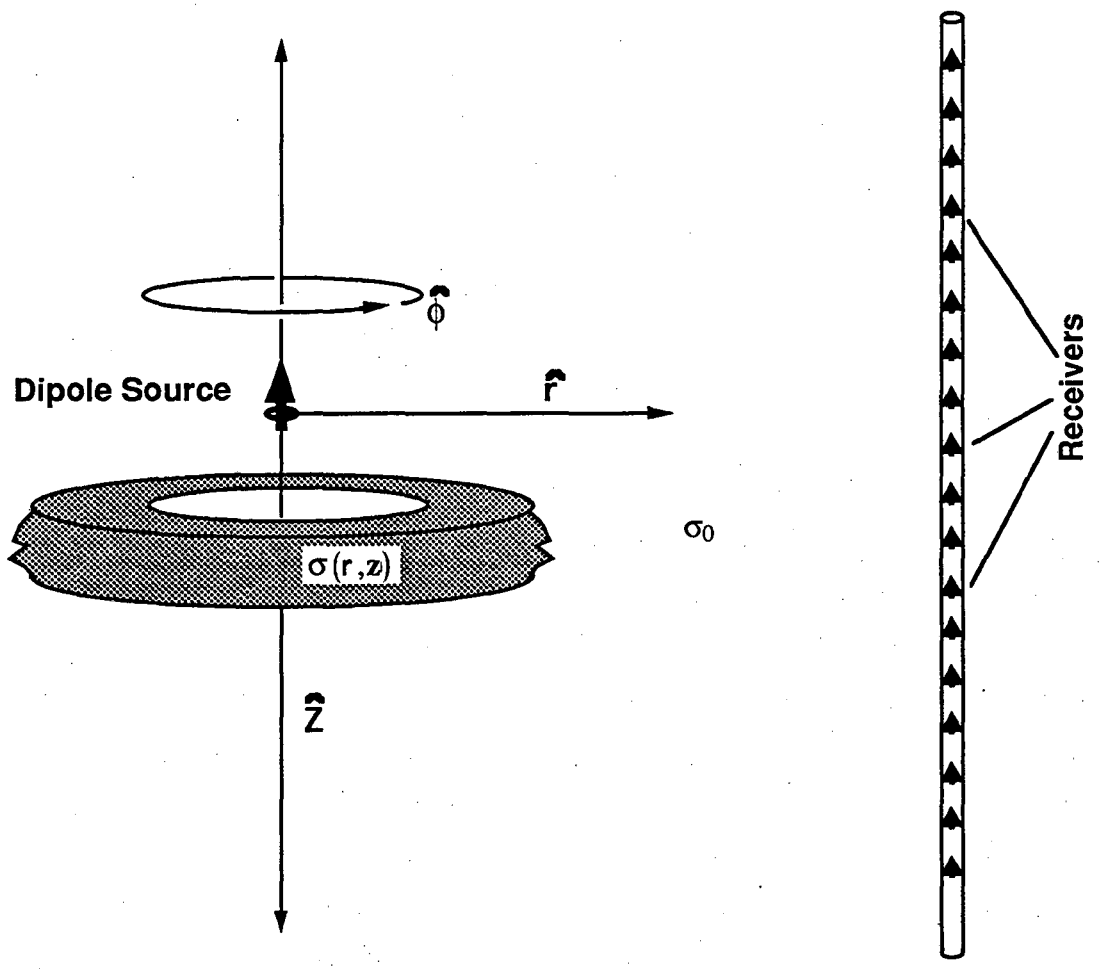

Figure 1. Cylindrical two-dimensional geometry for the crosswell problem. The inhomogeneous body is cylindrically symmetric about the magnetic dipole axis.

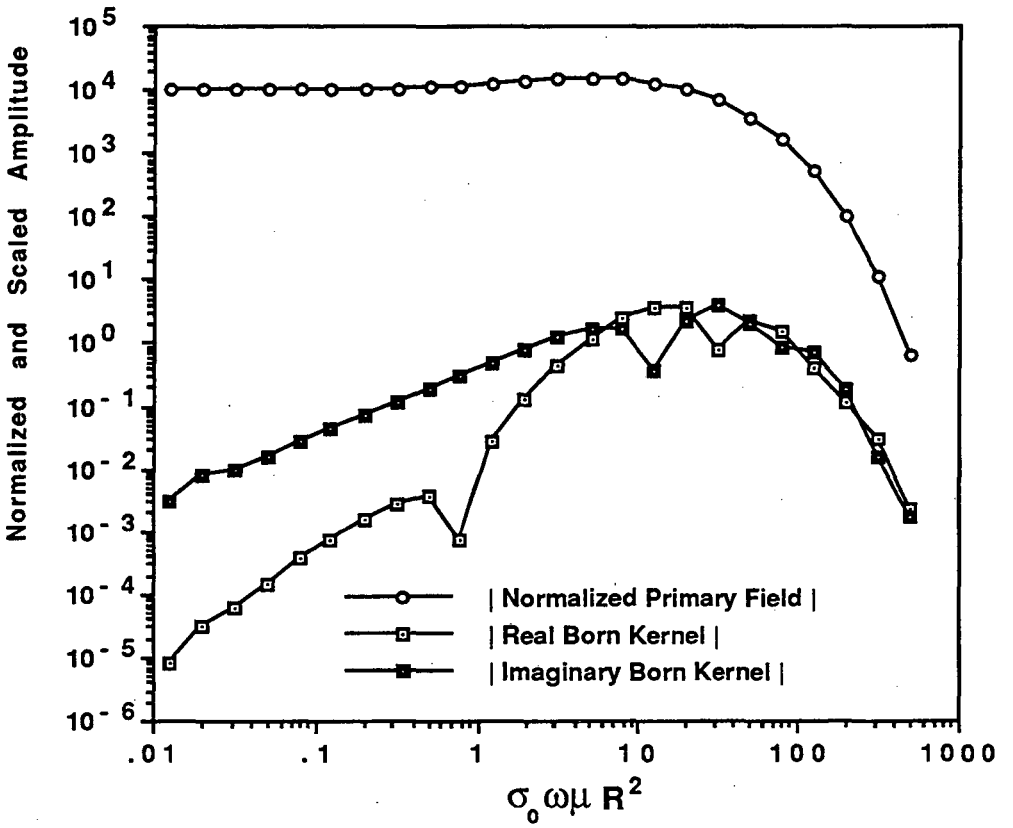

Figure 2. Plot of the Frechet derivative for coplanar magnetic dipoles.

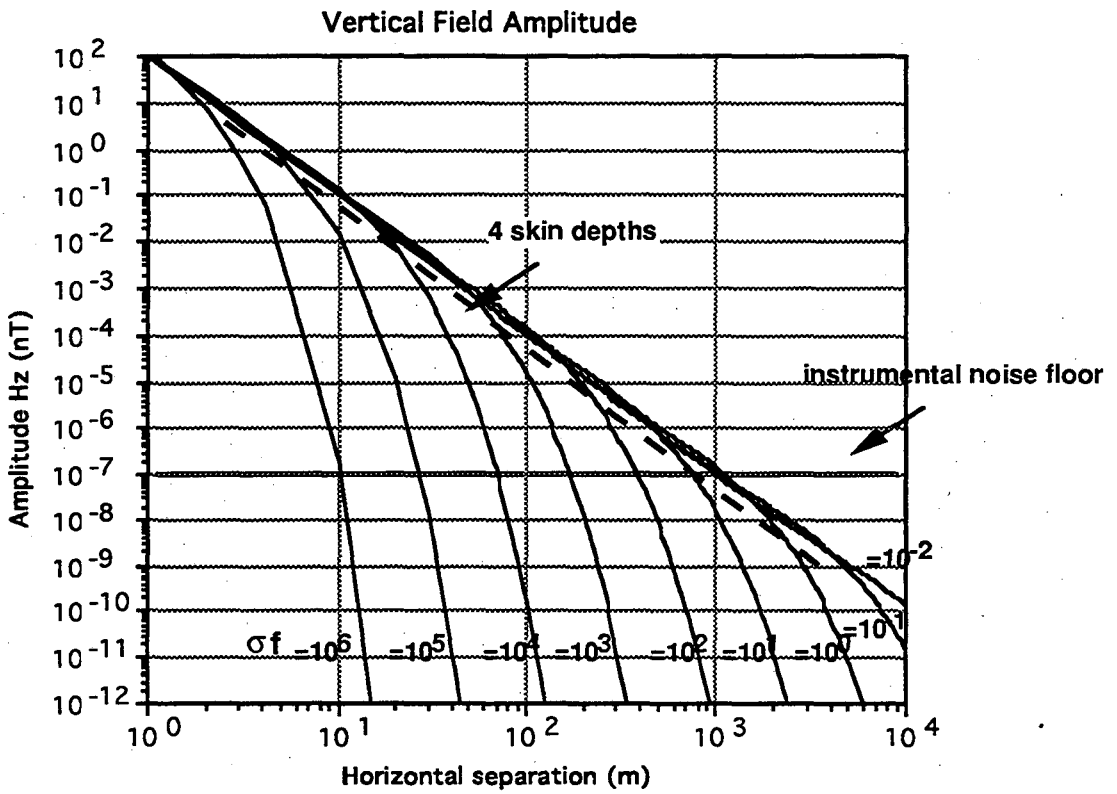

Figure 3. Vertical magnetic field amplitude for coplanar magnetic dipoles in a wholespace. Plots are for a range of frequency-conductivity products using a source moment of 1.

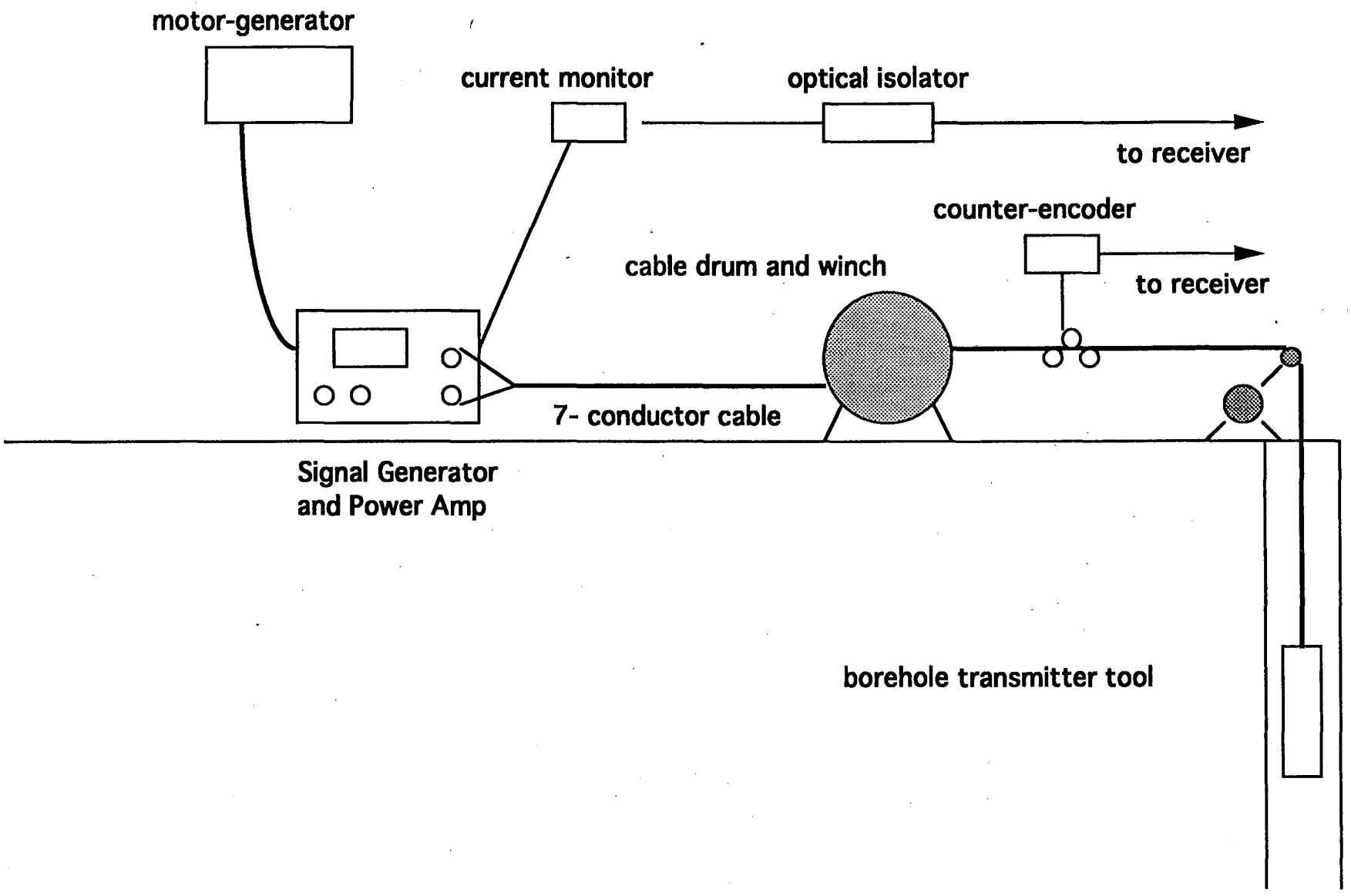

Figure 4. Schematic diagram of the crosshole EM transmitter.

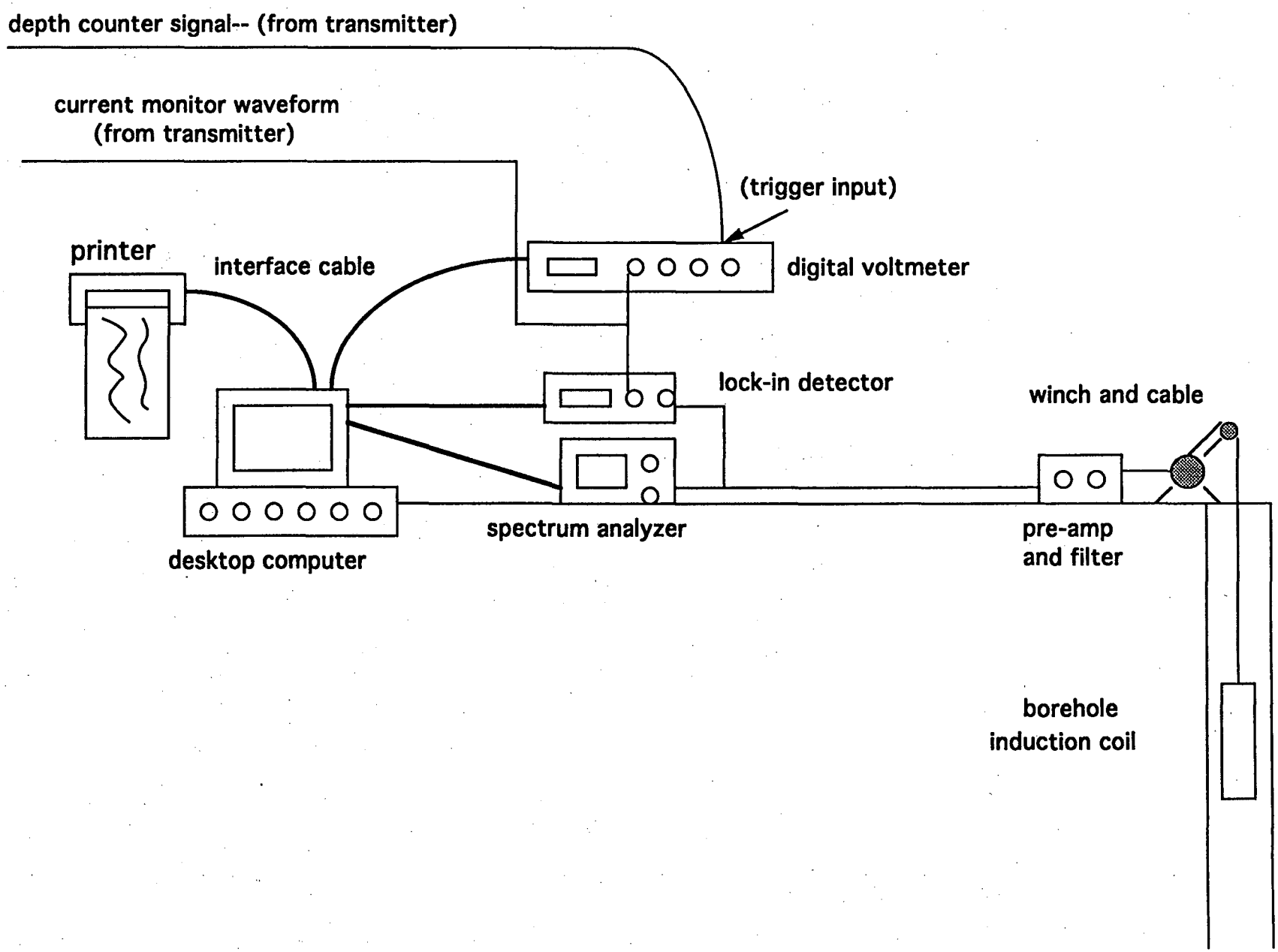

Figure 5. Schematic diagram of the crosshole EM receiver system.

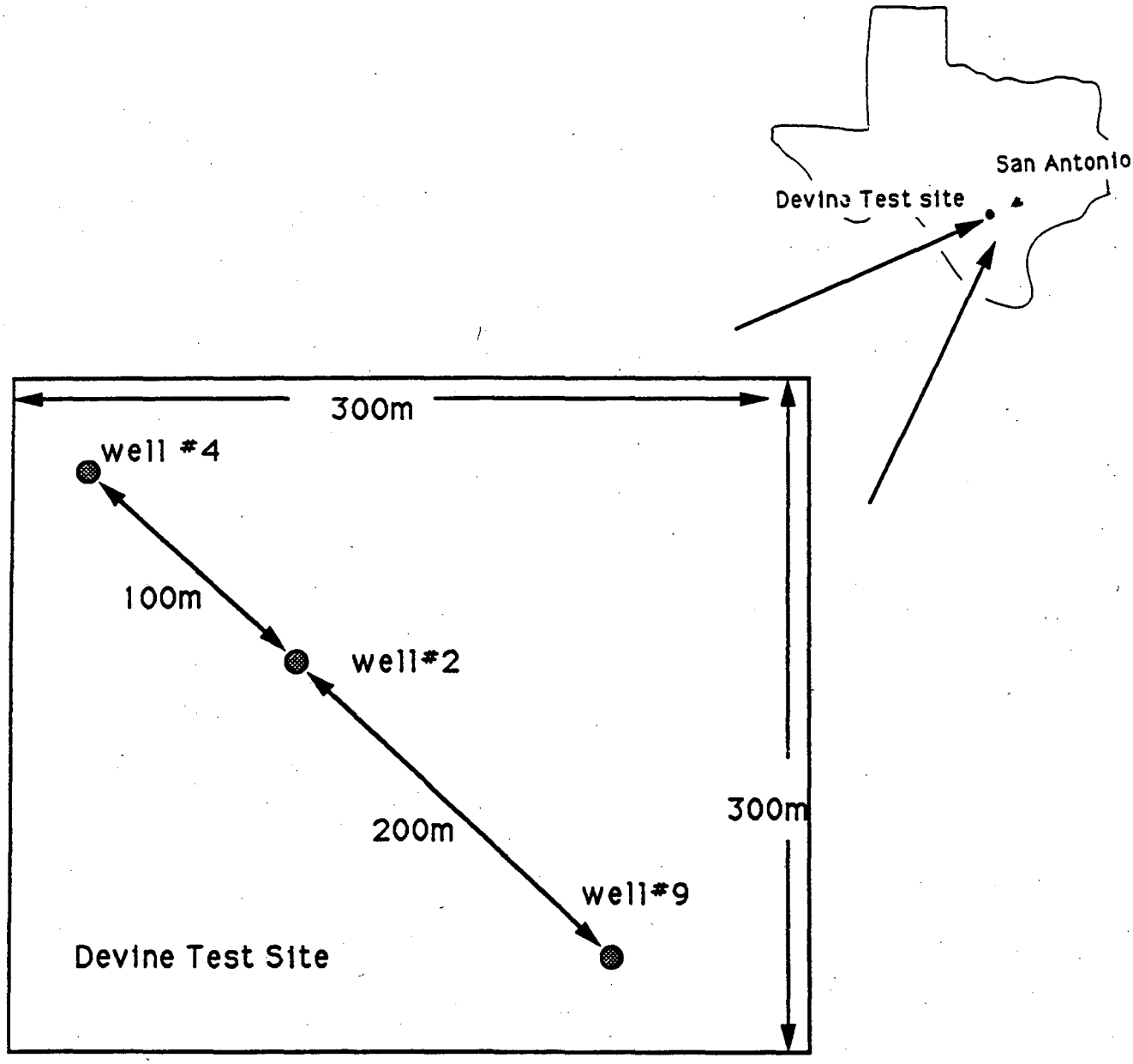

Figure 6. Location map for the Devine, Texas experimental facility.

Borehole Induction log from well # 4

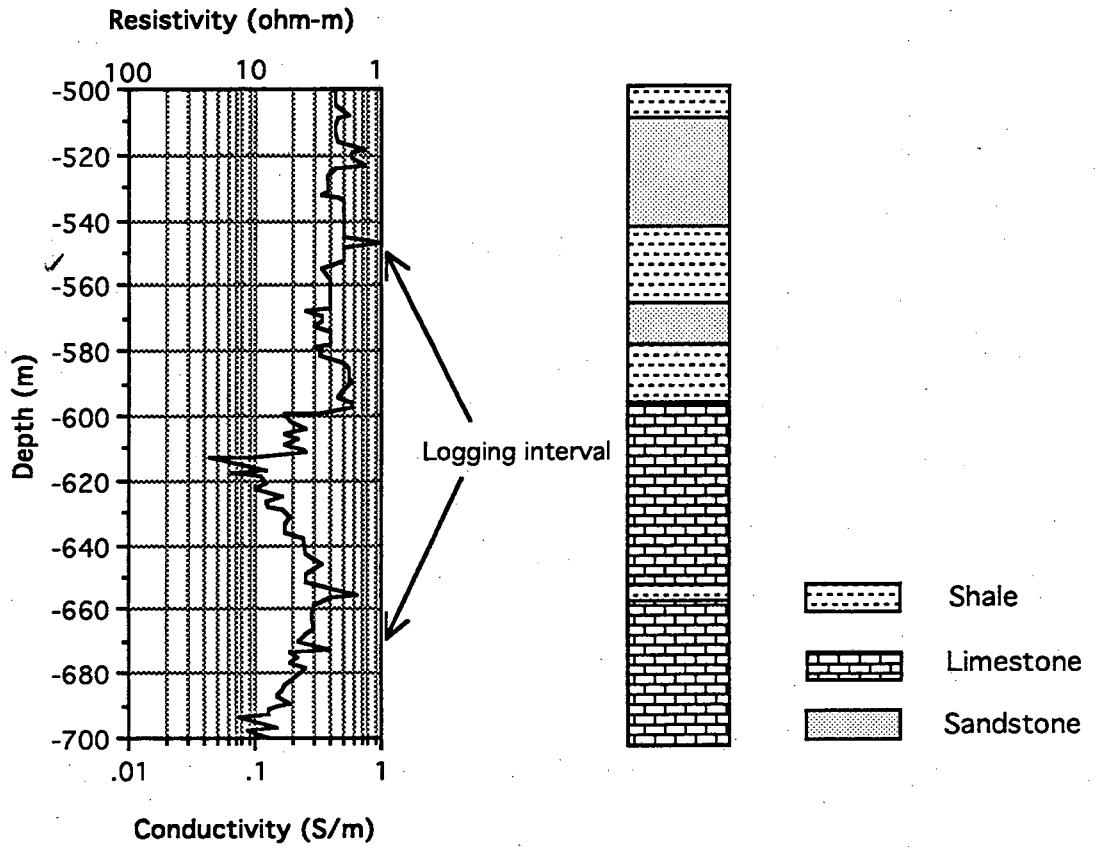

Figure 7. Geologic section and borehole induction log for the Devine test.

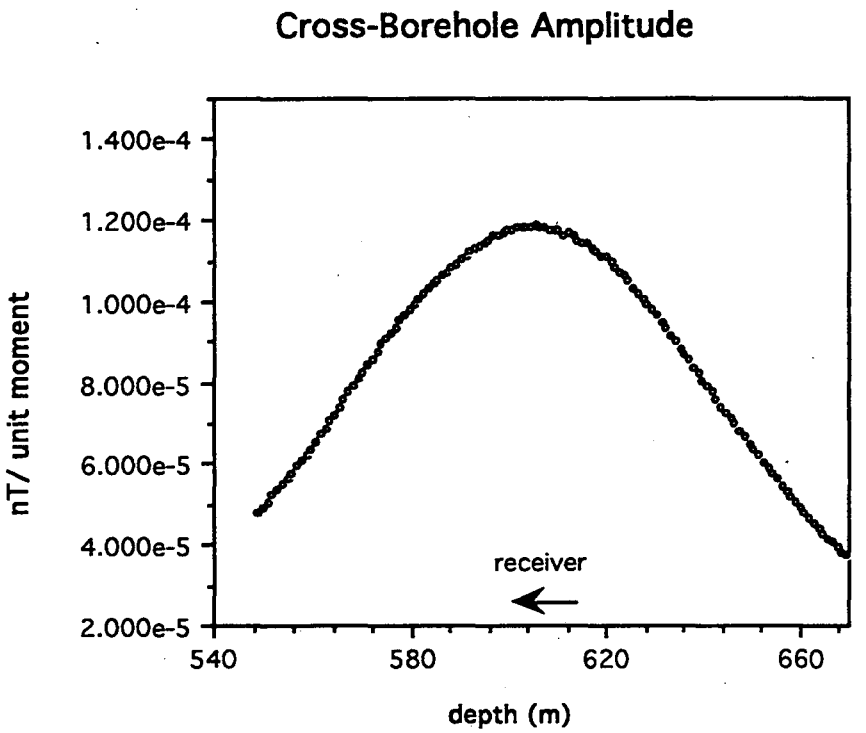

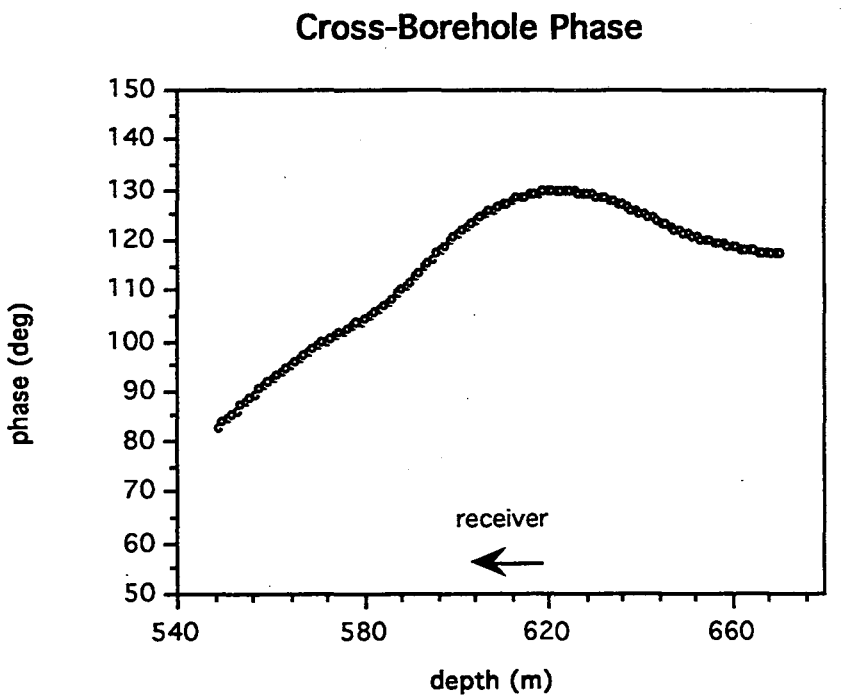

Figure 8. Sample cross-borehole amplitude and phase plots.

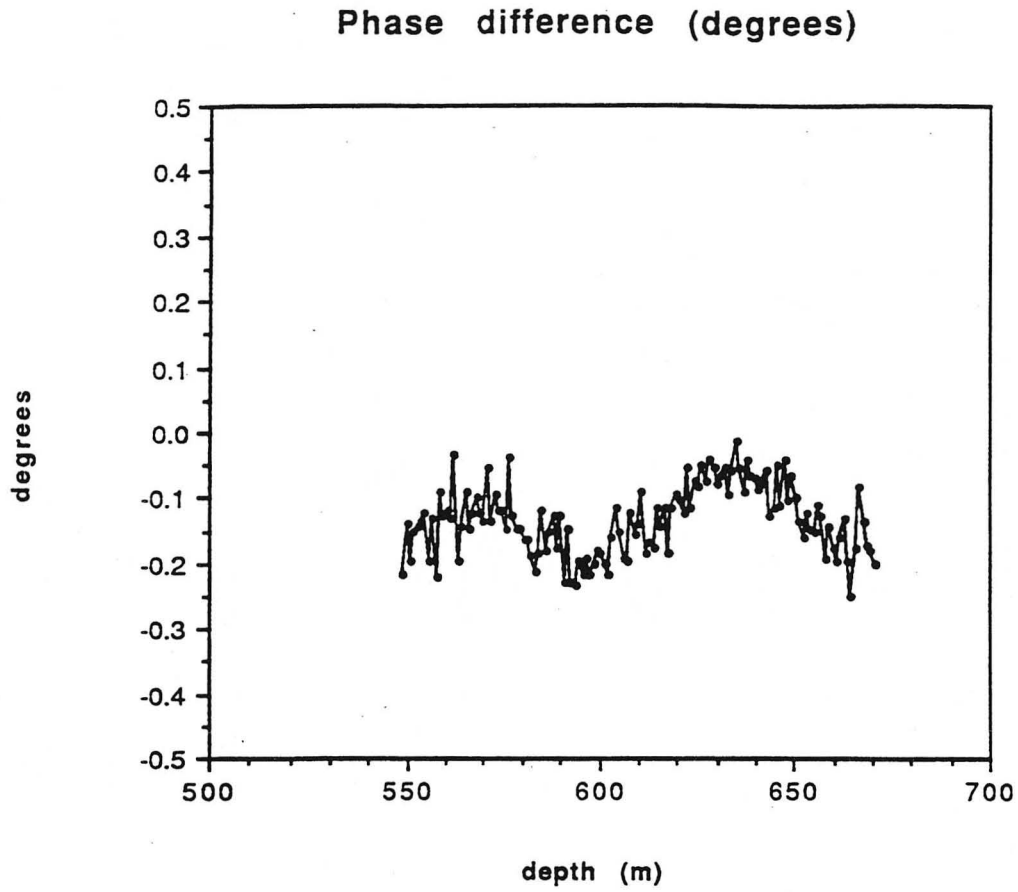

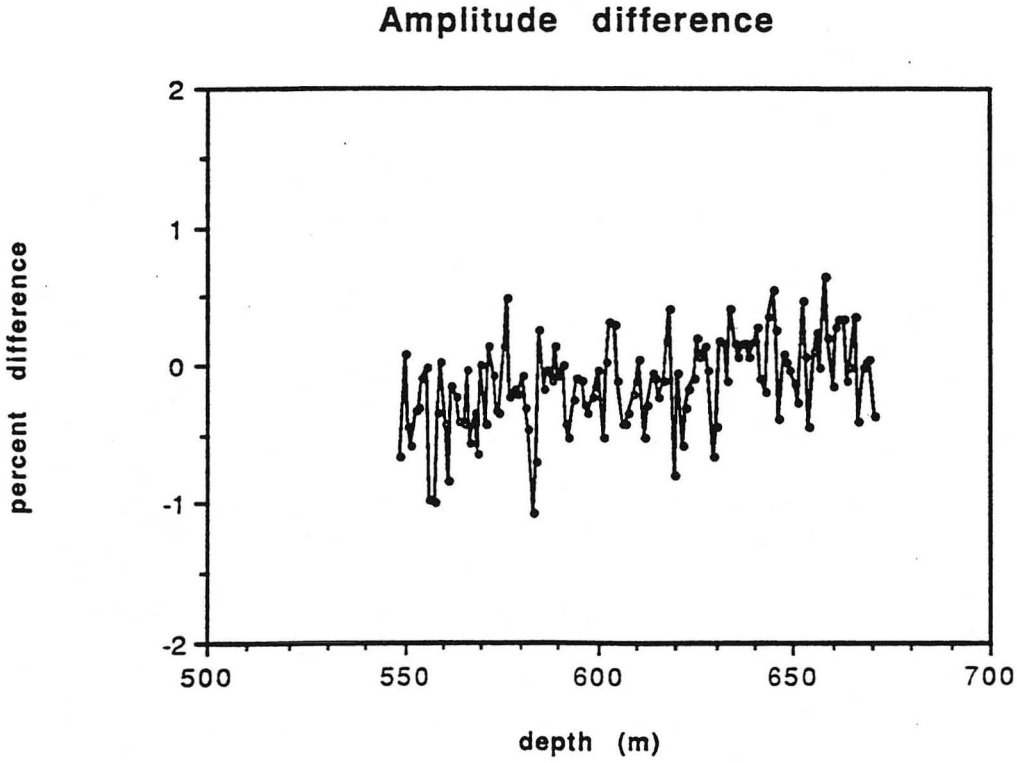

Figure 9. Percent difference of amplitude and phase difference (in degrees) for a 24 hour repeat test.

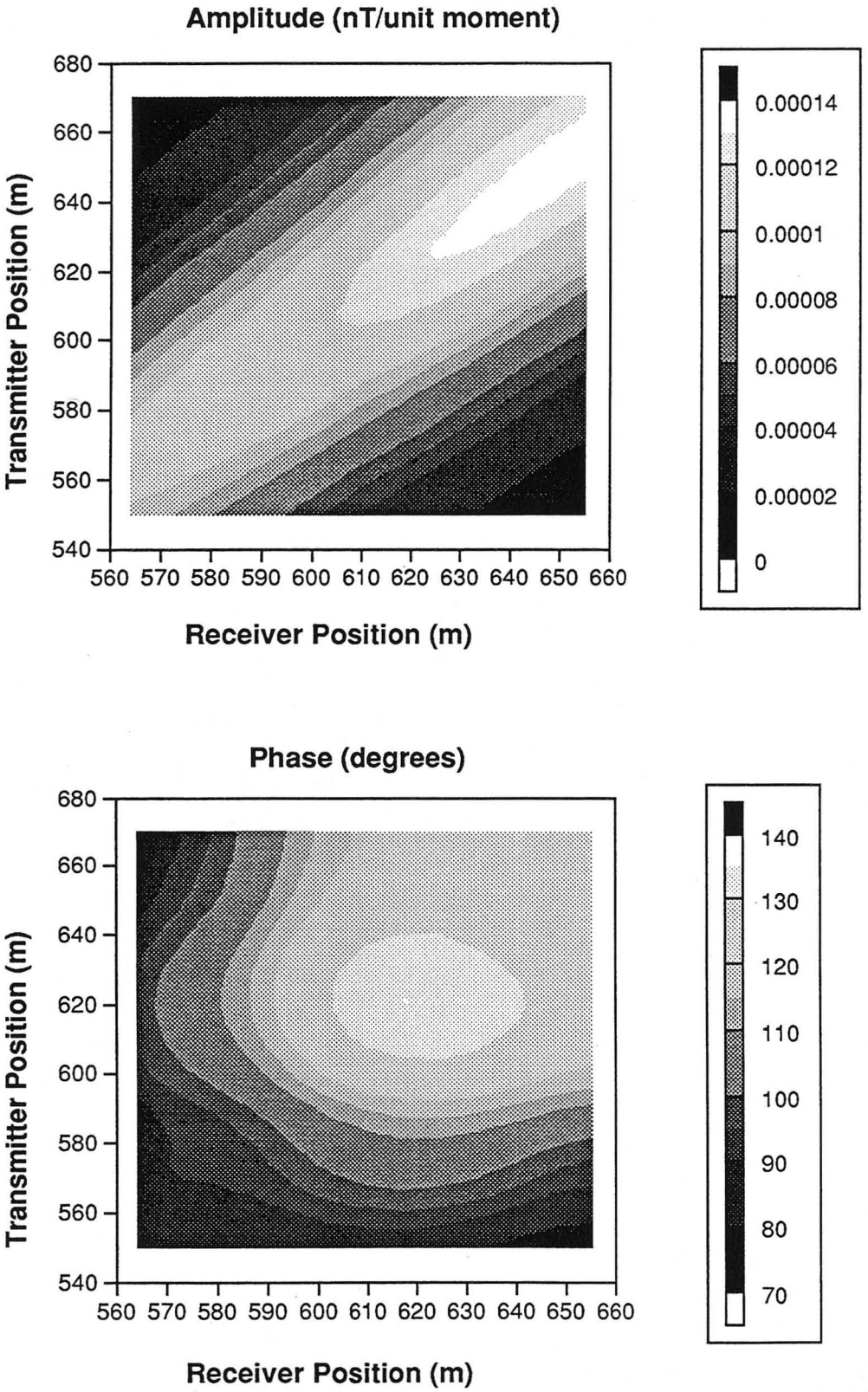

Figure 10. Contoured cross-borehole amplitude and phase data for the Devine survey.

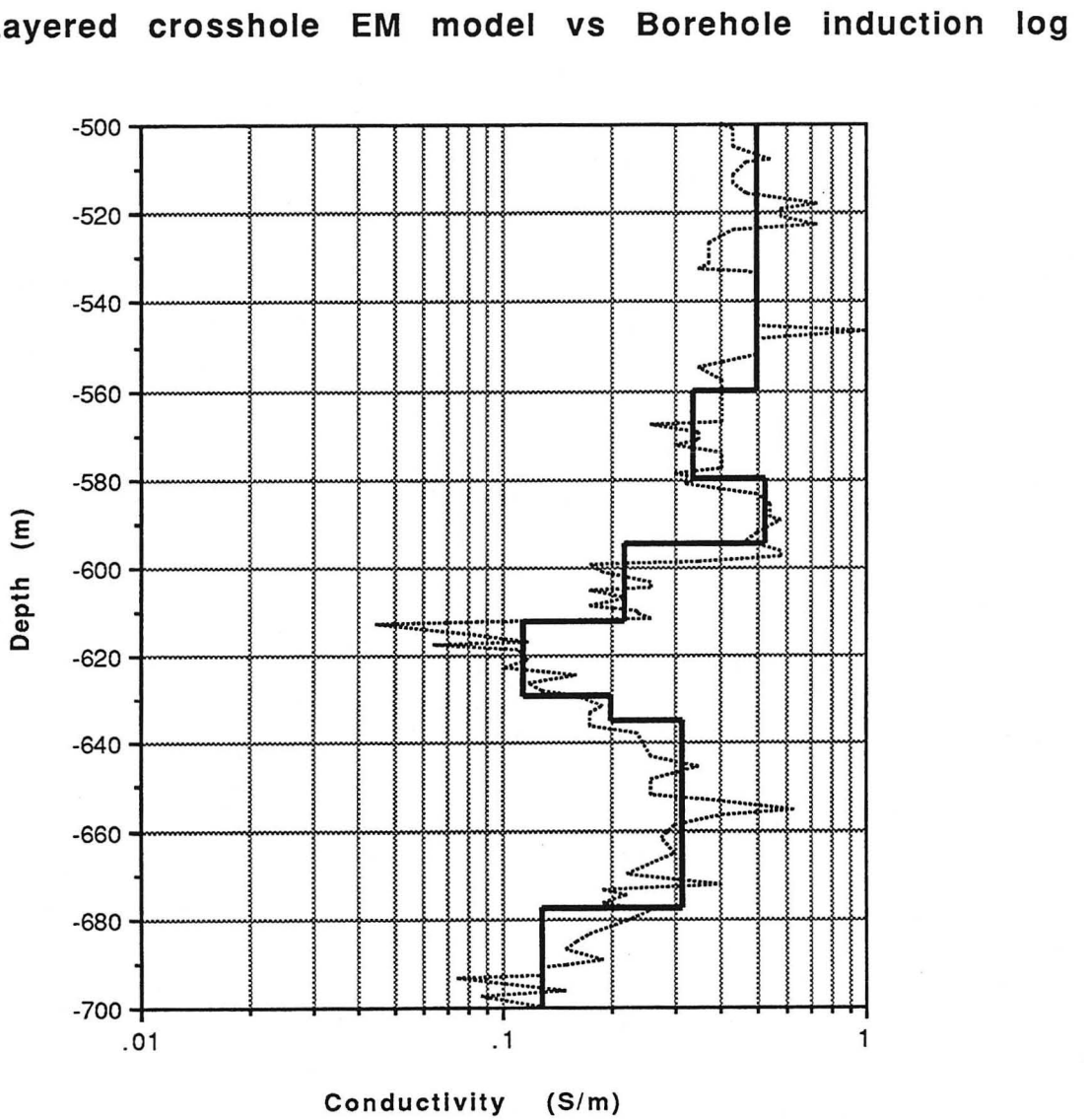

Figure 11. Comparison of the interpreted EM results and the borehole induction log in the same interval.

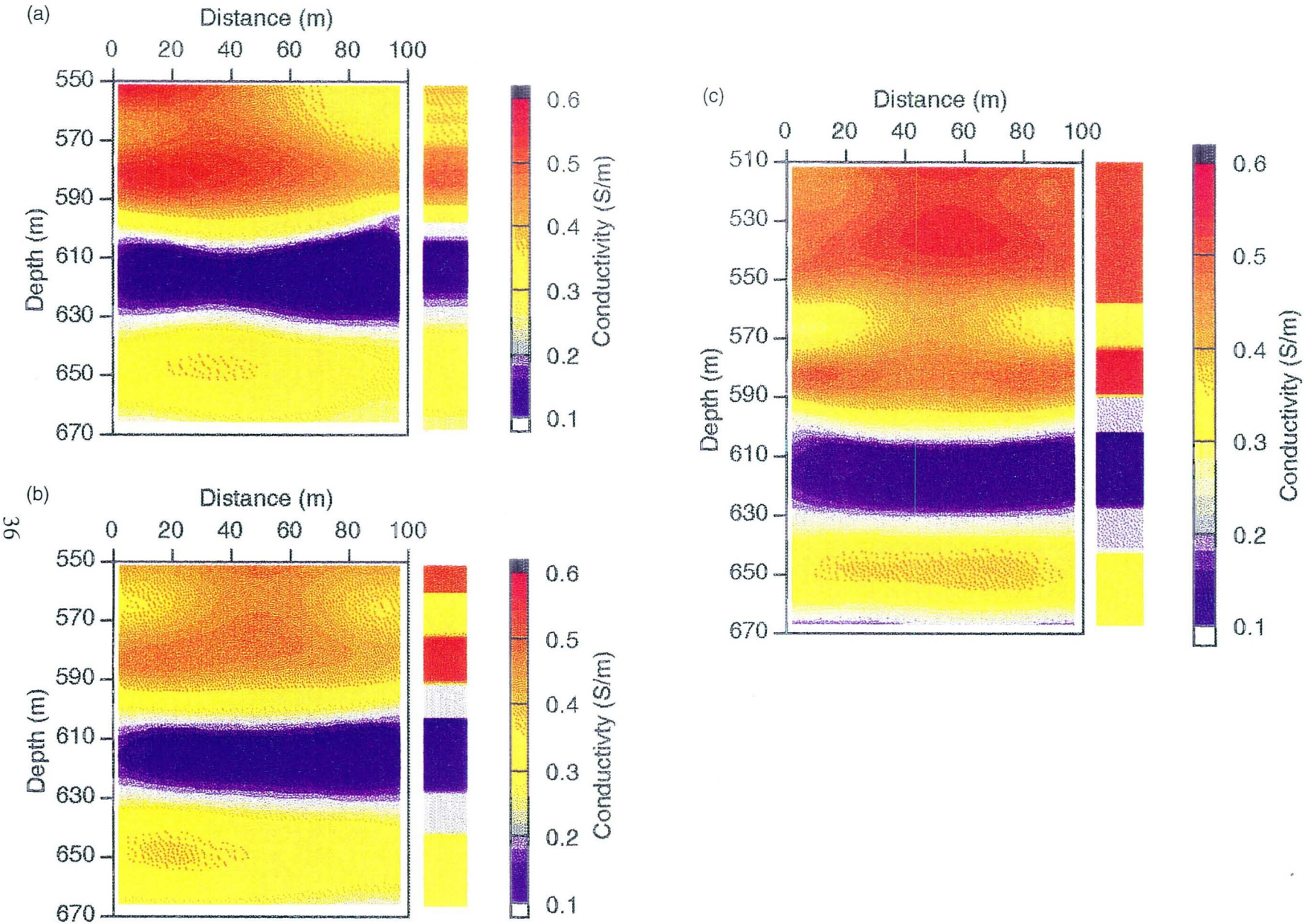

Figure 12. **(a)** Iterative Born image of the Devine crosshole EM results. **(b)** Iterative Born inversion using computer-generated data from a forward model. **(c)** Iterative Born inversion using computer-generated data and an extended measurement array.

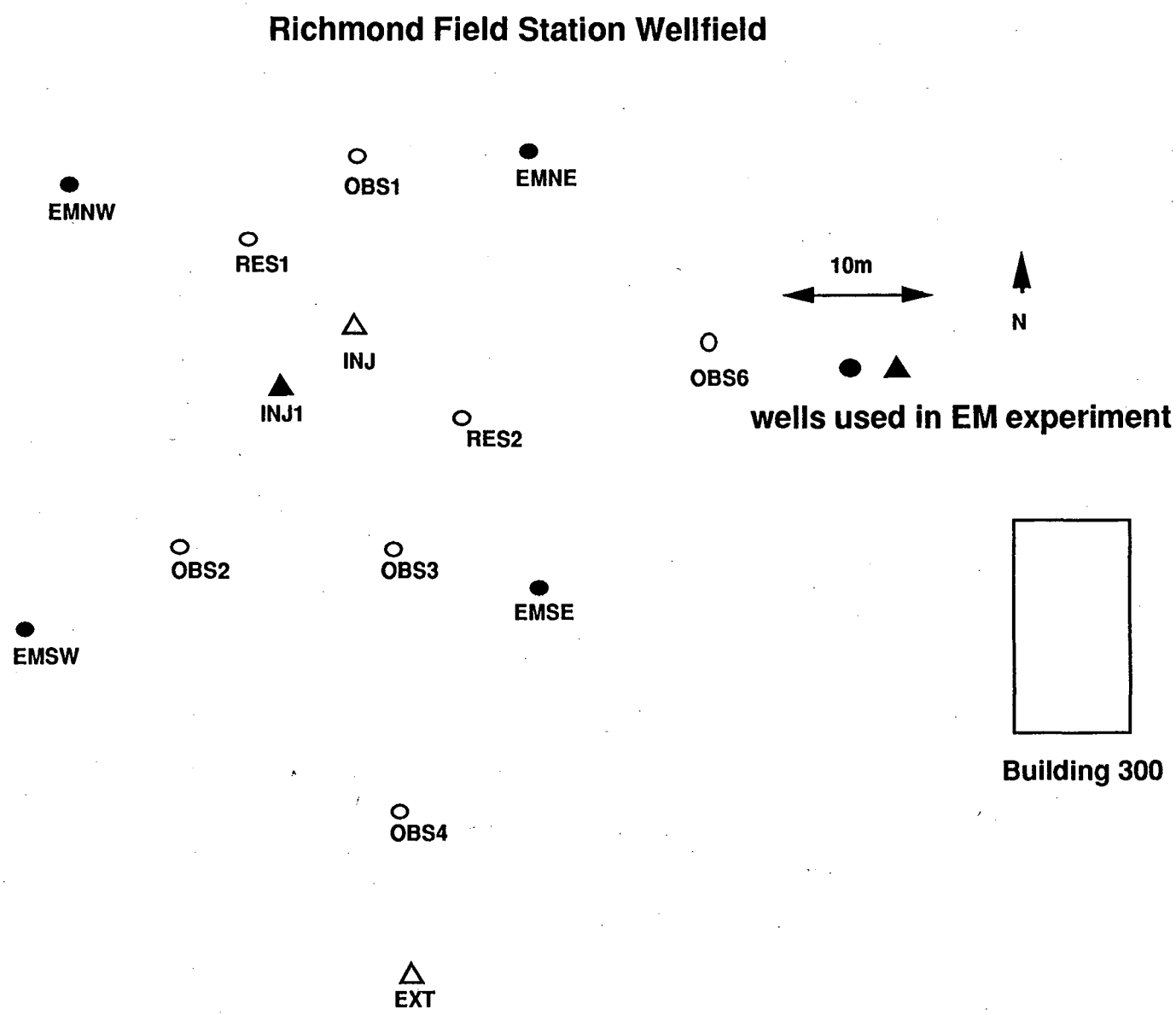

Figure 13. Plan view of the Richmond well field.

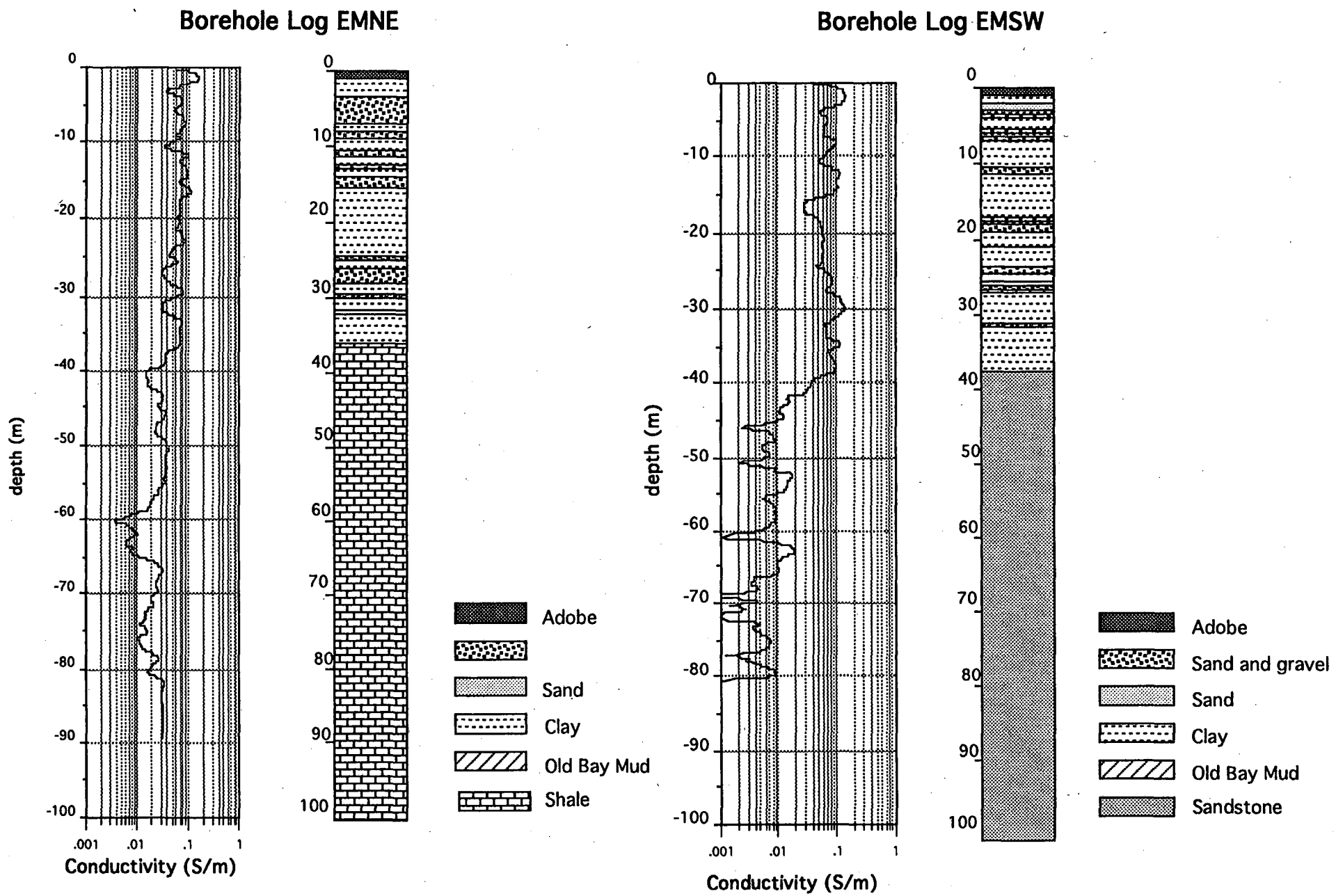

Figure 14. Borehole induction logs from well EMSW and EMNE at UC Richmond field station.

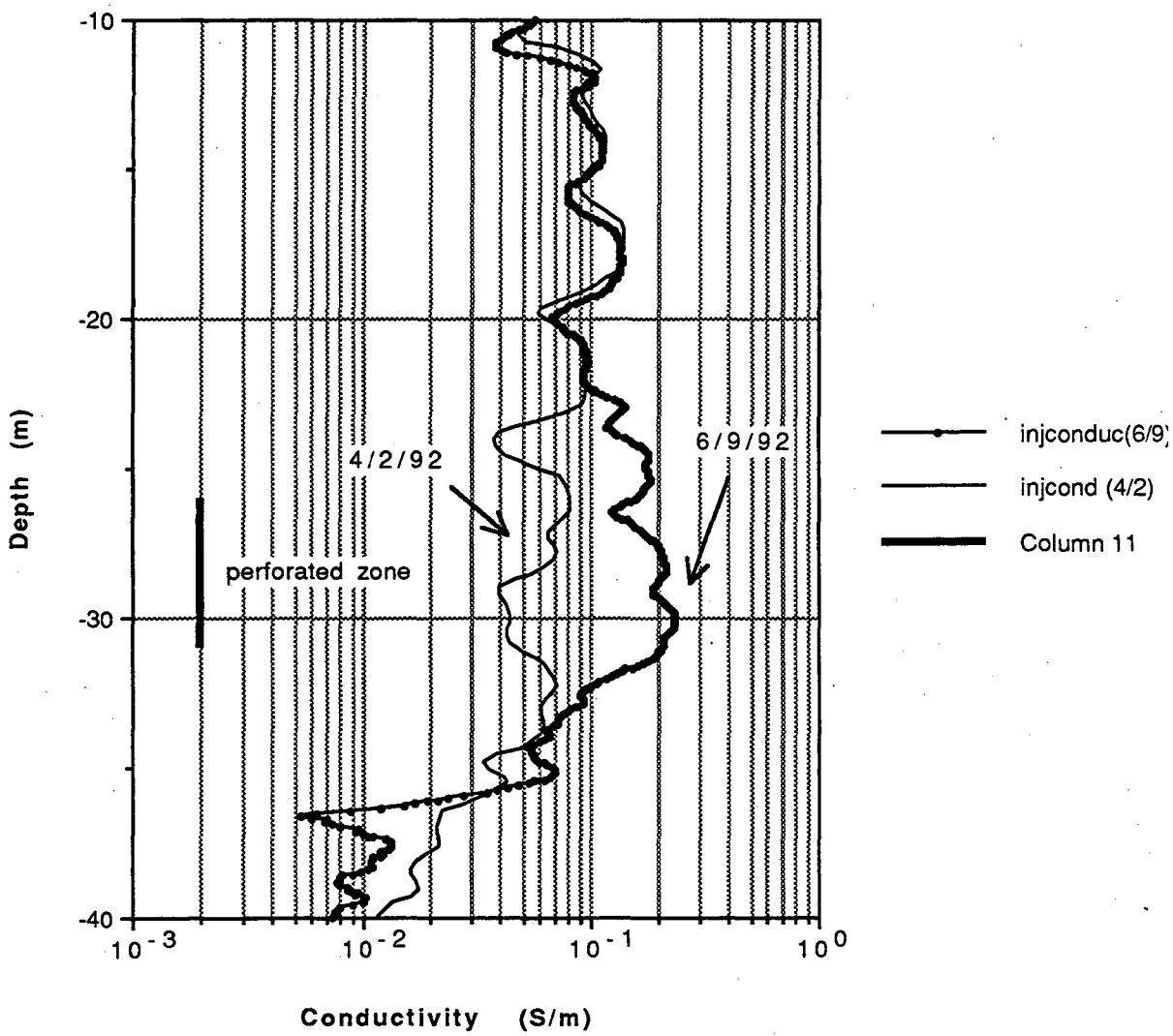

Figure 15. Borehole Induction logs in well INJ1 before and after saltwater injection.

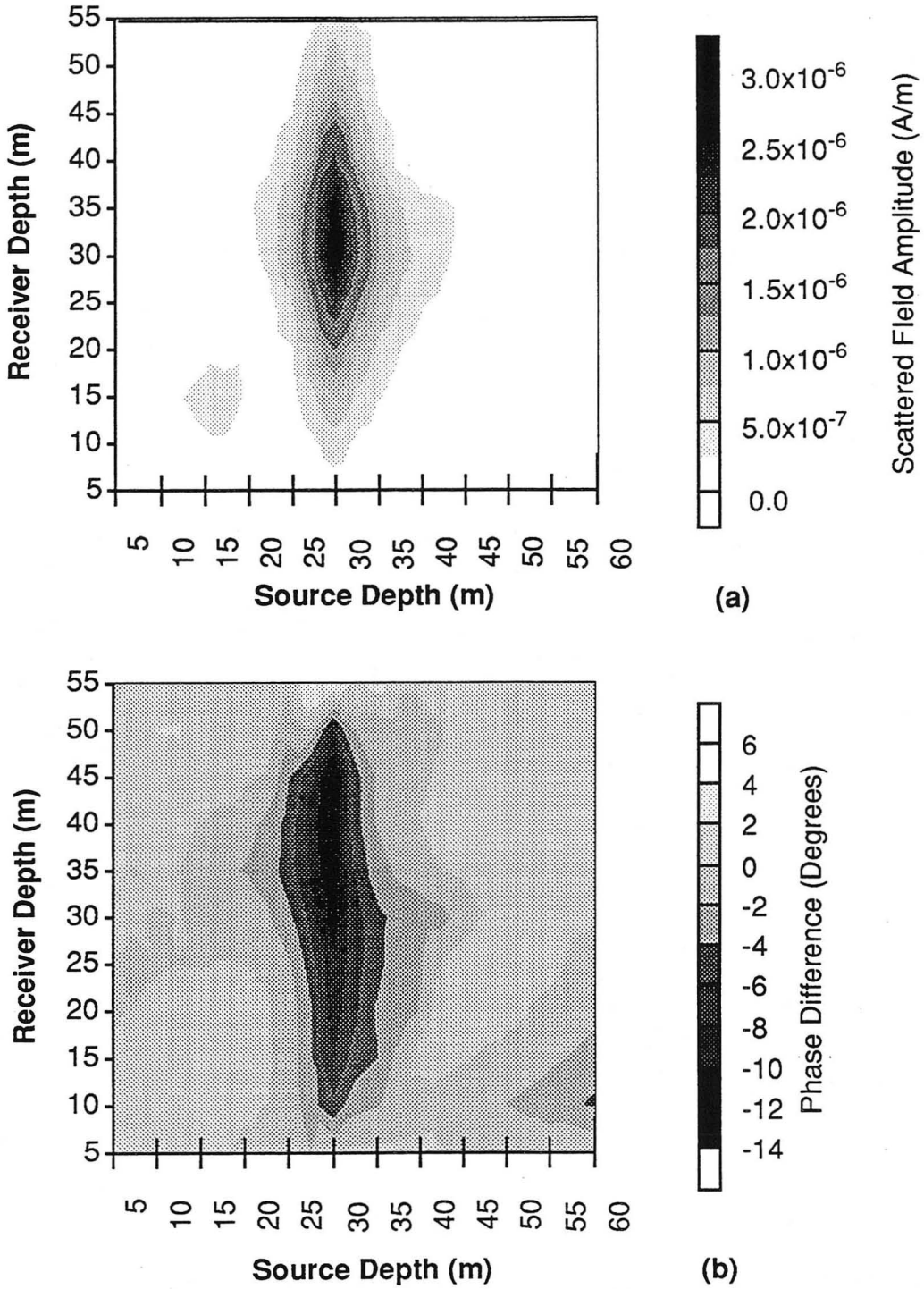

Figure 16. Secondary field differences from borehole EMNW before and after saltwater injection.

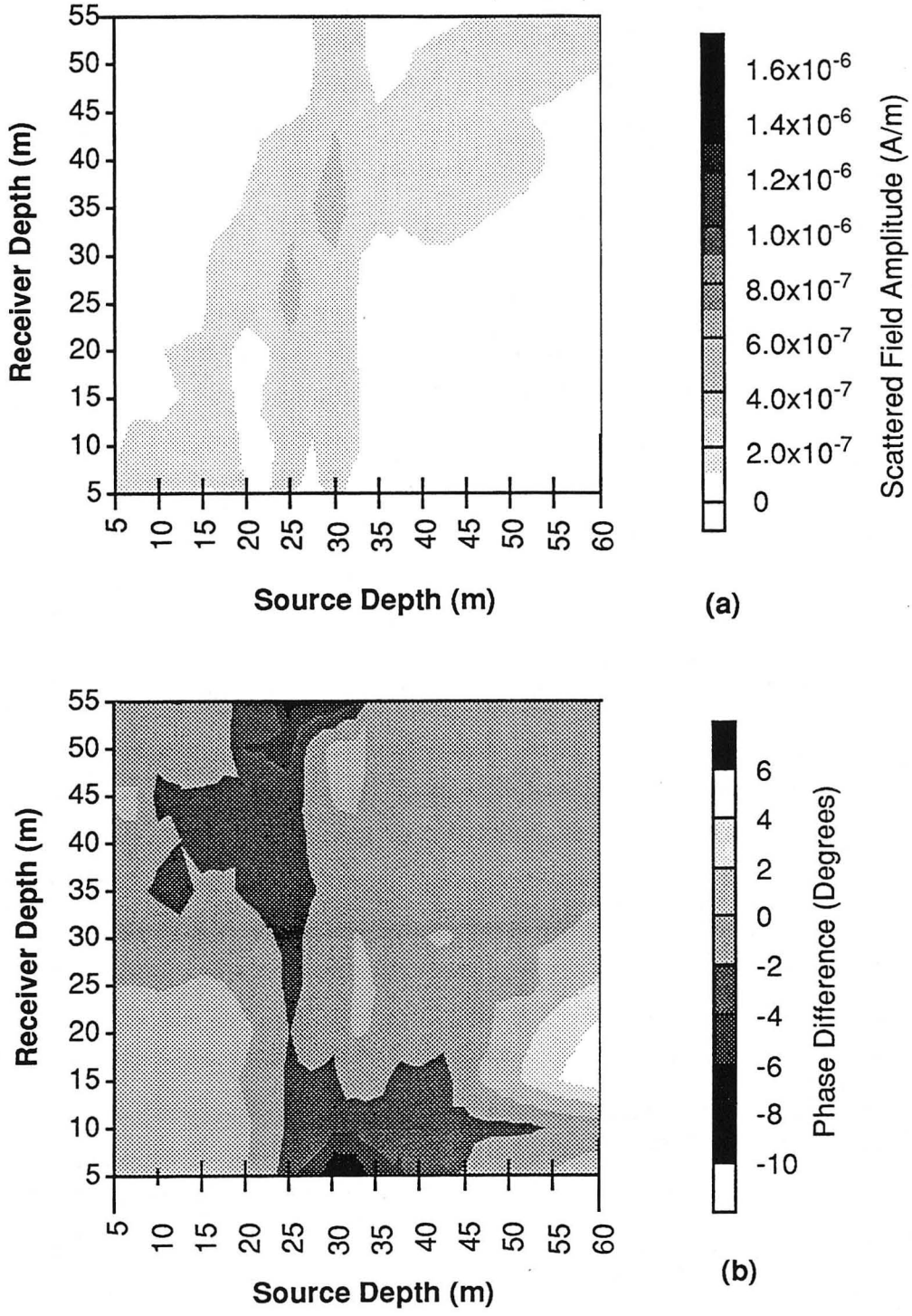

Figure 17. Secondary field differences from borehole EMSW before and after saltwater injection

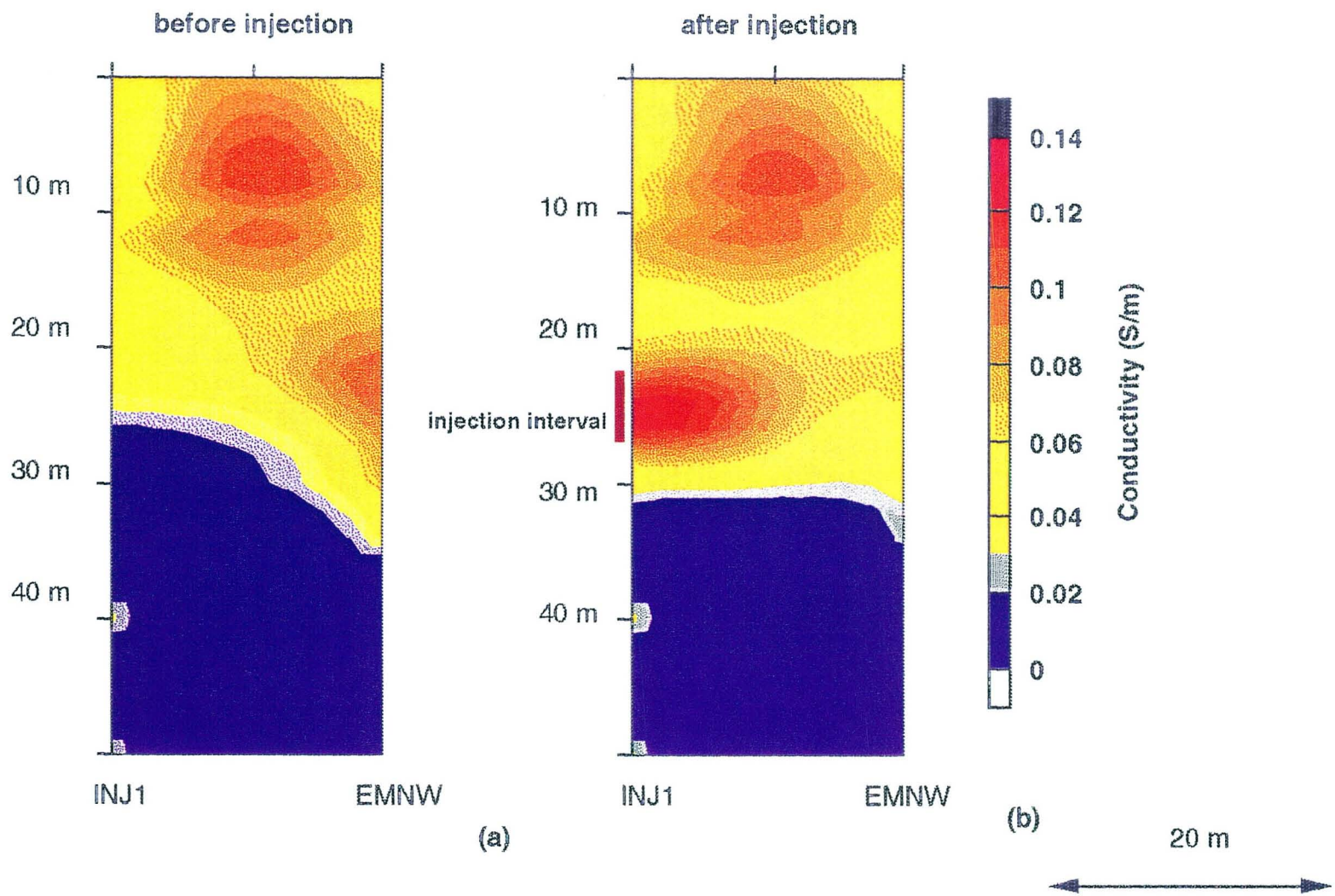

Figure 18. Tomographic inversion of EM profile INJ1-EMNW **(a)** before saltwater injection and **(b)** after saltwater injection.

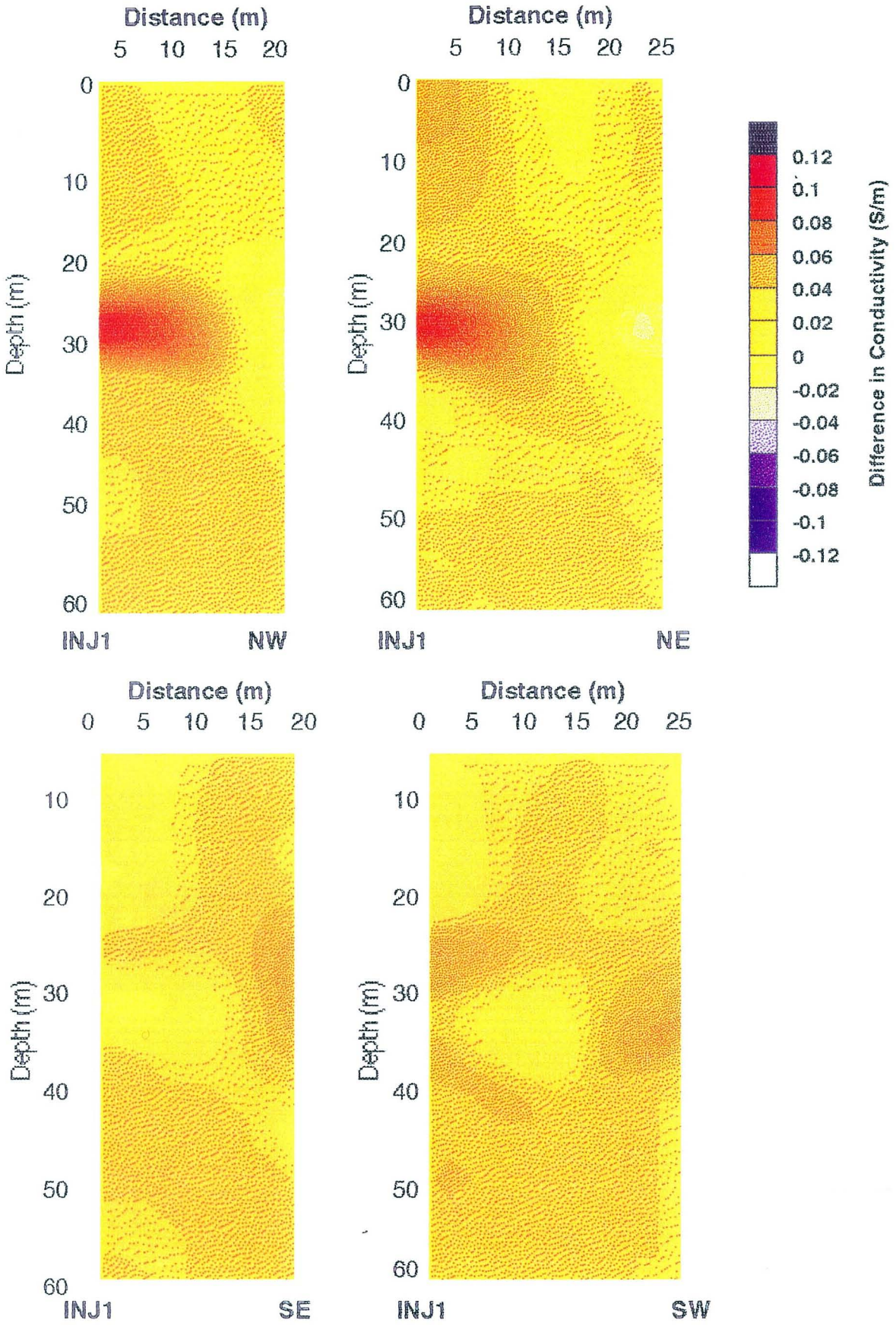

Figure 19. Difference images of the saltwater plume before and after injection for wells EMNW, EMNE, EMSW and EMSE.

LAWRENCE BERKELEY LABORATORY
UNIVERSITY OF CALIFORNIA
TECHNICAL INFORMATION DEPARTMENT
BERKELEY, CALIFORNIA 94720